



# Metal sorption to Spodosol Bs horizons: Organic matter complexes predominate

Charlotta Tiberg<sup>a, b</sup>, Carin Sjöstedt<sup>a</sup>, Jon Petter Gustafsson<sup>a, c, \*</sup>

<sup>a</sup> Department of Soil and Environment, Swedish University of Agricultural Sciences, Box 7014, SE-750 07, Uppsala, Sweden

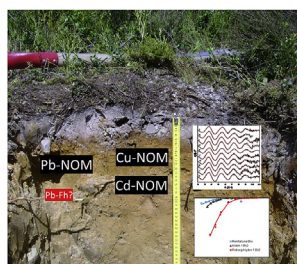
<sup>b</sup> Swedish Geotechnical Institute, Kornhamnstorg 61, SE-111 27, Stockholm, Sweden

<sup>c</sup> Department of Sustainable Development, Environmental Science and Engineering, KTH Royal Institute of Technology, Teknikringen 10B, SE-100 44, Stockholm, Sweden

## HIGHLIGHTS

- Organic matter complexes predominate cadmium(II), copper(II) and lead(II) sorption.
- An assemblage model with default parameter values did not succeed in 6 of 7 soils.
- The accessibility of organic matter was low due to its interaction with (hydr)oxides.
- Little or no lead(II) was bound to ferrihydrite, possibly due to allophane interference.

## GRAPHICAL ABSTRACT



## ARTICLE INFO

### Article history:

Received 26 October 2017

Received in revised form

22 December 2017

Accepted 2 January 2018

Available online 4 January 2018

### Keywords:

Cadmium

Copper

Lead

Soil

EXAFS

Assemblage model

## ABSTRACT

While metal sorption mechanisms have been studied extensively for soil surface horizons, little information exists for subsoils, for example Spodosol Bs horizons. Here the sorption of cadmium(II), copper(II) and lead(II) to seven Bs horizons from five sites was studied. Extended X-ray absorption fine structure (EXAFS) spectroscopy showed that cadmium(II) and lead(II) were bound as inner-sphere complexes to organic matter. Addition of *o*-phosphate (to  $1 \mu\text{mol l}^{-1}$ ) did not result in any significant enhancement of metal sorption, nor did it influence EXAFS speciation. An assemblage model using the SHM and CD-MUSIC models overestimated metal sorption for six out of seven soil samples. To agree with experimental results, substantial decreases (up to 8-fold) had to be made for the fraction 'active organic matter',  $f_{HS}$ , while the point-of-zero charge (PZC) of ferrihydrite had to be increased. The largest decreases of  $f_{HS}$  were found for the soils with the lowest ratio of pyrophosphate-to oxalate-extractable Al ( $Al_{pypp}/Al_{ox}$ ), suggesting that in these soils, humic and fulvic acids were to a large extent inaccessible for metal sorption. The low reactivity of ferrihydrite towards lead(II) can be explained by potential spillover effects from co-existing allophane, but other factors such as ferrihydrite crystallisation could not be ruled out. In conclusion, organic matter was the predominant sorbent for cadmium(II), copper(II) and lead(II). However, for lead(II) the optimised model suggests additional, but minor, contributions from Fe (hydr) oxide surface complexes. These results will be important to correctly model metal sorption in spodic materials.

© 2018 The Authors. Published by Elsevier Ltd. This is an open access article under the CC BY-NC-ND license (<http://creativecommons.org/licenses/by-nc-nd/4.0/>).

\* Corresponding author. Department of Soil and Environment, Swedish University of Agricultural Sciences, Box 7014, SE-750 07, Uppsala, Sweden.

E-mail address: [jon-petter.gustafsson@slu.se](mailto:jon-petter.gustafsson@slu.se) (J.P. Gustafsson).

## 1. Introduction

Knowledge on the sorption properties of soil materials is of crucial importance for risk assessments of metal-contaminated soils. A proper understanding of the mechanisms involved is a prerequisite for successful use of models that predict metal sorption. In recent years, a large body of evidence has been assembled concerning the sorption of cadmium(II), copper(II) and lead(II) to the surface horizon of soils. Some of the evidence were from so-called ‘assemblage models’ (Groenberg and Lofts, 2014) that assume that the total metal sorption is determined by additive contributions from individual sorbents (Davis et al., 1998). These models rely on mechanistically based models that describe sorption to individual components in the matrix. Examples include the NICA-Donnan (Kinniburgh et al., 1999), WHAM (Tipping et al., 2011) and SHM (Gustafsson, 2001) models for organic complexation, and the DLM (Dzombak and Morel, 1990) and CD-MUSIC (Hiemstra and van Riemsdijk, 1996) models for Fe/Al (hydr)oxide sorption.

For cadmium(II) and copper(II), the models suggest natural organic matter (NOM) to be the dominant sorbent of the surface horizons of temperate soils (Weng et al., 2001; Gustafsson et al., 2003; Shi et al., 2007). These conclusions were supported by results from EXAFS spectroscopy, showing a predominance of Cu-NOM complexes in many soils (Cancès et al., 2003; Flogeac et al., 2004; Martínez-Villegas and Martínez, 2008).

Lead(II) is bound comparatively strongly to ferrihydrite. Some model-based papers for soils suggested iron(III) (hydr)oxides to be important sorbents for lead(II) in soils and waters (e.g. Lofts and Tipping, 2000; Weng et al., 2001), whereas others emphasized binding to NOM (Gustafsson et al., 2003). Most assemblage models underestimate lead(II) sorption (Weng et al., 2002; Cancès et al., 2003; Groenberg and Lofts, 2014). This may be caused by a small number of previously unrecognized binding sites with high affinity for lead(II) (Gustafsson et al., 2011). Most spectroscopic studies show that organic matter is the single most important sorbent in many soils, although there are additional contributions from iron(III) or manganese(IV) oxides (Morin et al., 1999; Strawn and Sparks, 2001; Scheckel and Ryan, 2004).

So far, most metal sorption studies in soils have dealt with surface horizons, whereas subsoils, such as the Spodosol Bs horizon, have received relatively little attention. However, subsoil horizons can be important for risk assessments as they delay the transport of metals to ground and surface waters. Spodic materials are conceptually interesting as they contain large amounts of poorly crystalline iron(III) (hydr)oxide phases as well as allophane/ imogolite (Karlton et al., 2000). The few studies made on metal

sorption to Spodosol Bs horizons include the ones of Lumsdon (1996, 2004), who investigated Cd adsorption to some Scottish Spodosol B (probably Bs) horizons, and of Gustafsson et al. (2003), who included three Bs horizons in their modelling of metal sorption in Swedish soils. The latter authors found that in two of the B horizons the used assemblage model overestimated sorption, and it was hypothesized that humic substances were inactivated through adsorption to the oxide components. Until now, however, no systematic study has been undertaken to study the metal sorption properties of Spodosol Bs horizons.

Hence, the main objective of this work was to identify the predominant sorbent for added cadmium(II) and lead(II) in Spodosol Bs horizons, and to investigate whether assemblage models developed for surface horizons may be applicable also for Spodosol Bs horizons. An additional objective was to find out whether the presence of PO<sub>4</sub>-P (*o*-phosphate) could enhance metal sorption to Spodosol Bs horizons. In earlier work, we found that cadmium(II), copper(II) and lead(II) form ternary surface complexes with PO<sub>4</sub>-P and the surface of ferrihydrite under acidic conditions, which enhance metal binding (Tiberg et al., 2013; Tiberg and Gustafsson, 2016). To address these issues, EXAFS spectroscopy was used to unravel the binding mode of cadmium(II) and lead(II) in the Bs horizons. After a set of batch experiments, we also tested whether it was possible to simulate the sorption of cadmium(II), copper(II) and lead(II) correctly by use of assemblage modelling.

## 2. Materials and methods

### 2.1. Soils

Seven Bs horizon samples from five sites in south central Sweden were used in the investigation (Table 1). All sites were characterised by coniferous forest (*Picea abies* Karst. and/or *Pinus sylvestris* L.), and the soils were Typic Haplorthods (Soil Survey Staff, 2014). Klotten 1 Bs2, Risbergshöjden 1 Bs2, and Romfartuna Bhs were sampled in 1998 for a previous study (Gustafsson et al., 2003). In 2012, new samples were taken from Klotten and Risbergshöjden sites (Klotten 2 Bs and Risbergshöjden 2 Bs), and samples were collected also from the Risfallet and Tärnsjö sites.

Immediately after collection, the soil samples were sieved (<4 mm) and homogenized in their field-moist state. They were stored in a cold room (+5 °C) until further use. Subsamples for characterization were air-dried for a week at 30 °C. Batch experiments were carried out on the field-moist soils within six months of collection.

To quantify the concentrations of poorly crystalline Fe and Al (hydr)oxide phases, the soils were characterised by oxalate and

**Table 1**  
Selected soil chemical properties of the spodic B horizons studied<sup>a</sup>.

Sample	Location	Soil pH	Org. C %	Al <sub>ox</sub> mmol kg <sup>-1</sup>	Fe <sub>ox</sub>	Al <sub>pyp</sub>	Fe <sub>pyp</sub>	PSO <sub>4</sub>	Clay %	DOC mg L <sup>-1</sup>	PO <sub>4</sub> -P µg L <sup>-1</sup>
Klotten 1 Bs2	59.91°N	4.83	3.86	790	219	349	102	8.45	9	1.8	nd
Klotten 2 Bs	15.25°E	5.03	2.56	647	144	280	70	4.18	4	1.8	<1
Risbergshöjden 1 Bs2	59.72°N	5.94	0.80	519	74	43	1.3	8.56	5	<1	nd
Risbergshöjden 2 Bs	15.05°E	4.62	2.58	534	119	175	29	4.55	4	4.2	<1
Risfallet Bs	60.34°N 16.21°E	4.64	2.30	265	151	168	86	1.29	7	4.2	<1
Romfartuna Bhs	59.75°N 16.59°E	4.73	2.05	151	90	110	49	0.77	4	5.1	nd
Tärnsjö Bs	60.14°N 16.92°E	5.00	0.73	118	45	65	15	0.78	2	1.6	3.3

<sup>a</sup> The soil pH was measured in 0.01 M NaNO<sub>3</sub> (1:15 soil:solution ratio), Al<sub>ox</sub> = oxalate-extractable Al, Fe<sub>ox</sub> = oxalate-extractable Fe, Al<sub>pyp</sub> = pyrophosphate-extractable Al, Fe<sub>pyp</sub> = pyrophosphate-extractable Fe, PSO<sub>4</sub> = phosphate-extractable SO<sub>4</sub>, the given concentrations of DOC and PO<sub>4</sub>-P are the concentrations measured in 0.01 M NaNO<sub>3</sub> at the soil pH, nd = not determined.

pyrophosphate extractions (van Reeuwijk, 1995). The total organic C content was determined using a LECO CHN analyzer. Adsorbed  $\text{SO}_4$  was determined after extraction with  $0.02 \text{ mol L}^{-1} \text{ NaH}_2\text{PO}_4$  (Gustafsson et al., 2015).

## 2.2. Batch experiments

In all experiments, 2 g field-moist soil (3 g for Kloten 1 Bs2) was mixed with  $30 \text{ cm}^3$  solution in a polypropylene centrifuge tube with a screw cap. The centrifuge tubes were shaken for 6 d in a thermostat-controlled shaking water bath at  $8^\circ\text{C}$  (Kloten 1 Bs2, Risbergshöjden Bs2, and Romfartuna Bhs) or in an end-over-end shaker at  $20^\circ\text{C}$  (other soils). In all systems,  $0.01 \text{ mol L}^{-1} \text{ NaNO}_3$  was used as a background electrolyte. Varying additions of  $0.03 \text{ mol L}^{-1} \text{ HNO}_3$  or  $0.03 \text{ mol L}^{-1} \text{ NaOH}$  were made to produce a set of samples with different final pH values covering a range of pH from 4 to 6.5. Additions of metals were made using stock solutions of  $15 \text{ mmol L}^{-1} \text{ Cd}(\text{NO}_3)_2$ ,  $\text{Cu}(\text{NO}_3)_2$  and  $\text{Pb}(\text{NO}_3)_2$ . For Kloten 1 Bs2, Risbergshöjden Bs2 and Romfartuna Bhs, metals were added separately in different sets of experiments, whereas for the other soils they were added together. The final concentrations of added metal ranged from  $0.038$  to  $0.33 \text{ mmol kg}^{-1}$  for Cd, from  $0.38$  to  $1.64 \text{ mmol kg}^{-1}$  for Cu, and from  $0.34$  to  $1.64 \text{ mmol kg}^{-1}$  for Pb (c.f. details in Table S1 in Supplementary material).

To investigate the influence of  $\text{PO}_4\text{-P}$  on metal sorption,  $\text{PO}_4\text{-P}$  (from a  $15 \text{ mmol L}^{-1} \text{ NaH}_2\text{PO}_4$  stock solution) was added in a separate set of experiments to give a dissolved  $\text{PO}_4\text{-P}$  concentration of  $1 \mu\text{mol L}^{-1}$  after 6 d of shaking. This concentration level was chosen to represent a forest soil solution with a naturally high (but not very high) P concentration. The amount added P (shown in Table S1) was determined after preliminary experiments to obtain the  $\text{PO}_4\text{-P}$  sorption isotherm.

After 6 d of shaking, each tube was centrifuged, and the pH value was determined on the supernatant with a Radiometer combination electrode at the experimental temperature. The remaining supernatant was filtered through a  $0.2 \mu\text{m}$  single-use filter (Acrodisc PF) prior to analysis for major cations and metals (ICP-MS using a Perkin-Elmer ELAN 6100 instrument), DOC (using a Shimadzu TOC-5000 Analyzer),  $\text{PO}_4\text{-P}$  (using a Seal Analytical AA3 Auto-analyzer), and  $\text{SO}_4$  (using a Dionex, 2000i ion chromatograph).

## 2.3. EXAFS spectroscopy – sample preparation and measurements

Soil samples for EXAFS spectroscopy were prepared using identical procedures as described above, except that (i) the additions of cadmium(II) and lead(II) were slightly higher to ensure high-quality EXAFS results, and that (ii) the metals were not added together, but separately to different samples. For cadmium(II) the additions to the Kloten 2 and Risfallet samples were around  $2 \text{ mmol Cd kg}^{-1}$  (Table 2), which means that the molar ratio of Cd to organic C was close to 0.001. For lead(II) two different additions were made to the Kloten 2 sample, 2.3 and  $4.5 \text{ mmol Pb kg}^{-1}$  (Table 3), equivalent to Pb:organic C ratios of 0.001 and 0.002, respectively. In both cases,  $\text{PO}_4\text{-P}$  was added to separate samples using the same concentration levels as in the batch experiment. Additional samples were prepared in which As(V) as  $\text{NaH}_2\text{AsO}_4$  was added instead of  $\text{PO}_4\text{-P}$ . The idea was that any second-shell contribution of As to the EXAFS spectra would be easier to identify, as As is a heavier element than P.

To facilitate interpretation of soil spectra, standard spectra of  $0.5 \text{ mol L}^{-1}$  and  $15 \text{ mmol L}^{-1} \text{ Cd}(\text{NO}_3)_2$  solution and cadmium(II) bound to FA (Suwannee River Fulvic Acid, IHSS, St Paul, MN) were collected. The latter sample was prepared by mixing a stock solution of  $\text{Cd}(\text{NO}_3)_2$  with dissolved FA. The pH of the mixture was adjusted to pH 6.3 with  $0.1 \text{ M NaOH}$ , and was then left to equilibrate

for 24 h at the beamline until EXAFS analysis. This solution contained  $8 \text{ mM Cd}$  and  $8 \text{ g L}^{-1} \text{ FA}$ . A similar procedure was used to produce a standard spectrum of lead(II) bound to FA, except that the final solution contained  $3 \text{ mM Pb}$  and  $8 \text{ g L}^{-1} \text{ FA}$ . The final pH was 5.75.

The procedures for EXAFS measurements have been described in detail in previous papers (Tiberg et al., 2013 for Pb; Tiberg and Gustafsson, 2016 for Cd) and are therefore only briefly reiterated here. The EXAFS measurements at the Cd K edge at  $26,711 \text{ eV}$  were performed at beamline B18, Diamond Light Source, UK, for the soil samples, and at beamline X-11A, National Synchrotron Lightsource (NSLS), Brookhaven Laboratory, US, for the Cd solution standards and for the Cd-FA standard. Measurements were performed in fluorescence mode, internal energy calibration was made with a foil of metallic cadmium, and between 3 and 10 scans were collected per sample. Both beamlines were equipped with a Si[311] double crystal monochromator and with a 9-element Ge fluorescence (Diamond) or with a PIPS (NSLS) detector. For lead(II), the EXAFS measurements were made at the Pb  $\text{L}_3$  edge at  $13,035 \text{ eV}$  at beamline 4-1, Stanford Synchrotron Radiation Lightsource (SSRL), US. Measurements were performed in fluorescence mode, internal energy calibration was made with a foil of metallic lead, and between 10 and 20 scans were collected per sample. The beamline was equipped with a Si[220] double crystal monochromator and with a 13-element Ge fluorescence detector.

## 2.4. EXAFS data analysis

All EXAFS spectra were treated in the Athena software (version 0.8.061) (Ravel and Newville, 2005). Energy calibration, averaging and background removal were performed as described by Kelly et al. (2008). The background was removed using the AUTOBAK algorithm with a  $k$ -weight of two or three for the background function and  $\text{Rbkg} = 1$  for Cd and  $\text{Rbkg} = 1.1$  for Pb.

For the  $k^3$ -weighted Cd  $K$ -edge EXAFS spectra, wavelet transform (WT) analysis was performed (Funke et al., 2005; Chukalina, 2010) to differentiate between light (e.g. O, C, S) and heavy (e.g. Fe) elements (back-scatterers) in higher shells. The parameter combination  $\kappa = 7$  and  $\sigma = 1$  was employed, using a range of  $R + \Delta R$  from 2 to  $4 \text{ \AA}$  (corresponding to interatomic distances of about  $2.5\text{--}4.5 \text{ \AA}$ ). The  $k$ -ranges were the same as in the EXAFS fitting procedure.

The Artemis program (version 0.0.012) (Ravel and Newville, 2005) was used for final data treatment. Theoretical scattering paths were calculated with FEFF6 (Zabinsky et al., 1995). The amplitude reduction factor ( $S_0^2$ ) was set based on fitting of the first coordination shell. Several combinations of scattering paths were tested in the fitting procedure before deciding what paths to use. These included contributions from backscatterers in the first and second shells as well as multiple scattering paths.

Values of CN were chosen to give reasonable values of  $\sigma^2$ . Cd...C paths were calculated using FEFF6 (Zabinsky et al., 1995) based on a 5-member chelate ring structure. Possible second-shell contributions of Fe, As and P were considered (Tiberg et al., 2013; Tiberg and Gustafsson, 2016). The fitting was performed on the Fourier transform (FT) real part between 1 and  $4 \text{ \AA}$  (for Pb between 1.1 and  $4 \text{ \AA}$ ) using a Hanning window ( $dk = 1$ ) and optimization was over  $k$ -weights of 1, 2 and 3. Refined models were evaluated by the R factor in Artemis (goodness-of-fit parameter).

## 2.5. Geochemical modelling

The geochemical modelling platform Visual MINTEQ, version 3.1 (Gustafsson, 2016), was used. Speciation in solution was made with Visual MINTEQ's default thermodynamic database for aqueous

complexation, using the Davies equation for activity correction. To consider complexation to NOM, the Stockholm Humic Model (Gustafsson, 2001) was used, with modifications for solid-solution partitioning (Gustafsson and Kleja, 2005; complexation constants shown in Table S3). For lead(II) we considered the presence of specific high-affinity ligands in the solid phase (Gustafsson et al., 2011; Shi et al., 2013), but with one modification: instead of assuming a concentration of the high-affinity ligands of 0.2% of the total sites on HA (humic acid) and on FA, we calculated this number as 0.01% of the total organic C content. The resulting fits are similar to the ones presented by Gustafsson et al. (2011) for the data sets treated in that paper, and is in better conceptual agreement with the assumption that these ligands reside on a non-humic organic component.

In the modelling we assumed that there was no temperature effect on the metal-organic complexation reactions considered, i.e. that the reaction enthalpy was set to 0. There is an almost complete absence of data on the temperature dependence of these reactions (Tipping, 2002). The few data that exist suggest the thermodynamically induced temperature effect to be small (Rate, 2010).

We used the CD-MUSIC model as parameterized for ferrihydrite (Tiberg et al., 2013; Tiberg and Gustafsson, 2016) to simulate metal binding onto this soil component. Although allophane and other Al (hydr)oxide-type components are present in Spodosol Bs horizons (see, e.g. Karlton et al., 2000), they possess higher PZC:s (points-of zero charge) and in general they would be less likely to bind metals such as cadmium(II), copper(II) and lead(II); in addition there is no well-established surface complexation model for these sorbents.

To consider metal complexation to NOM using the SHM, it was assumed that 50% of the 'active' NOM in the solid phase consisted of HA, and 50% of FA. The dissolved organic matter (DOM) was considered fully active, dissolving only of FA (e.g. Gustafsson and Kleja, 2005; Gustafsson et al., 2011). As a starting point in the modelling it was assumed that  $f_{HS}$ , i.e. the fraction of solid-phase NOM that was active with respect to ion binding, was 0.55 (mean value of the soils studied by Gustafsson et al., 2003).

When using the CD-MUSIC model for ferrihydrite (complexation constants shown in Table S4), the content of ferrihydrite was calculated from oxalate extraction (Table 1), and the specific surface area was assumed to be  $650 \text{ m}^2 \text{ g}^{-1}$  as for freshly prepared 2-line ferrihydrite (Tiberg et al., 2013). As a starting point in the modelling we also assumed a PZC of 8.1 for the pure soil ferrihydrite phase (PZC(Fh) = 8.1), in agreement with freshly prepared ferrihydrite (Hiemstra, 2013). The surface charge characteristics of soil ferrihydrite may, however, be influenced by its co-occurrence with allophane in Spodosol Bs horizons. Karlton et al. (2000) reported that in two Bs horizons, there was a close intergrowth between ferrihydrite and a magnetically neutral material, probably allophane. In such associations, there may be a spillover of positively charged potential from the allophane component, which has a higher PZC (~10; Gustafsson, 2001). In one set of simulations we accounted for this effect in a simplified way, by changing the log  $K$ :s of the proton binding reaction (equal to the PZC) (Table S4).

In the modelling, the geochemically active metal concentration, as estimated by extraction with EDTA or dilute  $\text{HNO}_3$  (Table S2), was considered. However, as these concentrations were very low in the studied soils, the results were of little significance for the model results. The effect of major cations and anions ( $\text{Ca}^{2+}$ ,  $\text{Mg}^{2+}$ ,  $\text{K}^+$ ,  $\text{SO}_4^{2-}$ ) was considered by fixing the total dissolved concentrations at their measured values. Moreover, the effect of  $\text{Fe}^{3+}$  and  $\text{Al}^{3+}$  competition was considered by assuming equilibrium with respect to ferrihydrite ( $\log^*K_s = 2.69$  at  $25^\circ\text{C}$ ,  $\Delta H_r = -100.5 \text{ kJ mol}^{-1}$ ; Liu and Millero, 1999) and  $\text{Al}(\text{OH})_3(\text{s})$  ( $\log^*K_s = 8.29$  at  $25^\circ\text{C}$ ,  $\Delta H_r = -105.0 \text{ kJ mol}^{-1}$ ; Gustafsson et al., 2001), and by use of the van't Hoff approximation to recalculate these equilibrium constants

to  $8^\circ\text{C}$  and to  $20^\circ\text{C}$ , as needed.

### 3. Results and discussion

#### 3.1. EXAFS spectroscopy

The EXAFS spectra for cadmium(II) adsorbed to Kloten 2 Bs and Risfallet Bs were very similar in shape (Fig. S1, Supplementary materials), regardless of whether phosphate or arsenate was added or not. They also resembled the spectrum for cadmium(II) adsorbed to fulvic acid (Cd-FA), indicating that the cadmium(II) was bound in a similar way in all samples. The spectra of Cd adsorbed to ferrihydrite (Cd-Fh and Cd-P-Fh in Fig. S1) had a slightly different shape, for example at  $k = 7-8$ . Shell fitting of the EXAFS spectra was consistent with cadmium(II) being coordinated to six oxygens in the first shell (Table 2). The WT of the spectra (Fig. S2) was similar for data and models, suggesting that the model used was correct and that heavy elements such as P, Fe and As in the second shell could be excluded. Second-shell contributions were well modelled with 1.5 carbon atoms between 3.09 and 3.16 Å, implying that the bulk of the sorbed Cd was bound to NOM predominantly to oxygen-containing ligands such as carboxylate groups.

These results are comparable to the ones of Karlsson et al. (2005), although these authors claimed a significant involvement of thiols to the Cd coordination on NOM. However, in the current study there were no evidence for a significant first-shell contribution from S at ~2.5 Å, as shown both by shell fitting (Table 2; Fig. S1) and by the WT results (Fig. S2). Moreover, if thiols are significant contributors to Cd binding, the FT real part is affected (Fulda et al., 2013). The FT real part was, however, well described by the model (Fig. S3), and the patterns were similar to the one for carboxylate-bound Cd by Fulda et al. (2013). Hence, multiple evidence suggest a predominance of Cd bound as an inner-sphere complex to carboxylate ligands, although a minor contribution from thiol-bound Cd cannot be ruled out.

As is often the case, the quality of the Pb  $L_3$  EXAFS spectra only allowed a relatively small  $k$  range to be modelled, leading to results that are somewhat less clear than those for Cd. However, also for lead(II) the EXAFS spectra were consistent, suggesting an important role of organic ligands for lead(II) binding in the Kloten 2 Bs samples, also for those samples to which  $\text{PO}_4\text{-P}$  or As(V) had been added. The Pb  $L_3$  EXAFS spectra of the soil samples were similar in shape to those of the Pb-FA standard, but different from the ferrihydrite standards (Fig. S4), and shell fitting showed no clear evidence of heavy backscatters such as P, Fe and As (Table 3). Instead, for the soil samples, there was a second-shell contribution from O, or more probably, C, at around 3.08 Å. This agrees with the second-shell Pb...C distance of the soil studied by Strawn and Sparks (2001). Interestingly the Pb...C distance of Pb-FA was slightly longer, i.e. 3.25 Å. This path length agrees with earlier studies in which lead(II) was reacted with HA or FA (Xia et al., 1997; Xiong et al., 2013). The Pb-O and Pb...C distances observed are consistent with a predominance of strong Pb-NOM inner-sphere complexes in all studied soil samples (Xia et al., 1997; Strawn and Sparks, 2001). The difference in Pb...C path length could indicate a difference in lead(II)-NOM coordination between soil and FA, but the poorly resolved nature of the Pb...C interaction does not allow clear conclusions. Hence, the EXAFS results show a predominance of organic matter complexes also for lead(II). However, given the relatively poor quality of the Pb  $L_3$  edge EXAFS spectra, it cannot be excluded that Pb bound to Fe and Al (hydr)oxide phases was present to a minor extent.

Although only the Kloten 2 Bs soil was analysed by Pb  $L_3$  edge EXAFS, it should be noted that this sample had a relatively high content of oxalate-extractable Fe and Al (Table 1) and that,

**Table 2**  
Summary of shell fit results: cadmium(II) K-edge EXAFS of soil samples and standards. Parameters in italics were constrained during fitting.

Sample	Path	CN	R (Å)	$\sigma^2$ (Å <sup>2</sup> )	$\Delta E$ (eV)	$S_0^2$	R-factor (%)
Kloten 2 Cd 2.3 mmol kg <sup>-1</sup> Cd pH 6.12	Cd–O	6	2.28 (0.01)	0.010 (0.000)	1.92 (0.81)	0.90	0.48
	Cd···C	1.5	3.13 (0.04)	0.018 (0.005)			
	Cd–O–O	18	4.71 (0.06)	0.020	k-range 3.5–9.5		
Kloten 2 Cd+P 2.3 mmol kg <sup>-1</sup> Cd 11.4 mmol kg <sup>-1</sup> P pH 5.85	Cd–O	6	2.28 (0.01)	0.010 (0.000)	2.19 (0.63)	0.90	0.33
	Cd···C	1.5	3.16 (0.03)	0.012 (0.004)			
	Cd–O–O	18	4.79 (0.05)	0.020	k-range 3.5–9.5		
Kloten 2 Cd+As 2.3 mmol kg <sup>-1</sup> Cd 11.4 mmol kg <sup>-1</sup> As(V) pH 6.15	Cd–O	6	2.27 (0.01)	0.012 (0.000)	1.92 (0.74)	0.90	0.33
	Cd···C	1.5	3.09 (0.04)	0.014 (0.004)			
	Cd–O–O	18	4.65 (0.06)	0.020	k-range 3.5–9.5		
Risfallet Cd 1.9 mmol kg <sup>-1</sup> Cd pH 5.64	Cd–O	6	2.28 (0.01)	0.009 (0.000)	2.54 (0.78)	0.90	0.49
	Cd···C	1.5	3.15 (0.04)	0.013 (0.005)			
	Cd–O–O	18	4.70 (0.06)	0.019	k-range 3.5–9.5		
Risfallet Cd+As 1.9 mmol kg <sup>-1</sup> Cd 4.8 mmol kg <sup>-1</sup> As(V) pH 6.15	Cd–O	6	2.28 (0.00)	0.009 (0.000)	2.11 (0.49)	0.90	0.20
	Cd···C	1.5	3.15 (0.02)	0.008 (0.002)			
	Cd–O–O	18	4.73 (0.04)	0.019	k-range 3.5–9.5		
Cd(II)(aq) 0.5 0.5 M Cd(NO <sub>3</sub> ) <sub>2</sub>	Cd–O	6	2.27 (0.006)	0.008 (0.000)	2.87 (0.58)	0.65	0.70
	Cd–O–O	18	4.40 (0.033)	0.017			
	Cd–O···O	24	3.70 (0.10)	0.025	k-range 3–10		
Cd(II)(aq) 0.015 15 mM Cd(NO <sub>3</sub> ) <sub>2</sub>	Cd–O	6	2.27 (0.01)	0.008 (0.000)	0.70 (0.62) (0.47)	1	0.66
	Cd–O–O	18	4.43 (0.03)	0.017			
	Cd–O···O	24	3.72 (0.10)	0.025	k-range 3–10		
Cd-FA 8 mM Cd 8 g L <sup>-1</sup> FA pH 6.32	Cd–O	6	2.27 (0.005)	0.007 (0.000)	1.57 (0.64)	0.80	0.39
	Cd···C	2	3.12 (0.03)	0.013 (0.04)			
	Cd–O–O	18	4.67 (0.05)	0.014	k-range 3.4–10		
Cd-Fh 30 μM Cd <sup>2+</sup> 0.3 mM Fe pH 7.42	Cd–O	6	2.26 (0.01)	0.009 (0.001)	–0.37 (0.61)	0.75	0.7
	Cd···Fe1	0.5	3.26 (0.05)	0.006 (0.006)			
	Cd···Fe2	1	3.74 (0.04)	0.006 (0.005)			
Cd–P-Fh 30 μM Cd <sup>2+</sup> , 60 μM P 0.3 mM Fe pH 7.42	Cd–O	6	2.27 (0.01)	0.010 (0.000)	–0.10 (0.47)	0.85	0.4
	Cd···P	1	3.38 (0.04)	0.012 (0.007)			
	Cd···Fe2	1	3.80 (0.05)	0.013 (0.008)			
	Cd–O–O	18	4.50 (0.04)	0.020	k-range 2.6–9.5		

CN = Coordination number; R = Atomic distance;  $\sigma^2$  = Debye-Waller factor;  $\Delta E$  = Energy shift parameter;  $S_0^2$  = Passive amplitude reduction factor; R = R-factor = Athena goodness-of-fit parameter. Uncertainties of fitted parameters as given in Artemis (Ravel and Newville, 2005).

Added concentrations of cadmium(II), phosphate and arsenate are listed below the sample name.

The  $\sigma^2$  (Å<sup>2</sup>) of Cd–O–O (multiple scattering paths) were defined as 2<sup>\*</sup> $\sigma^2$  (Å<sup>2</sup>) for the Cd–O paths.

For each sample the  $\sigma^2$  (Å<sup>2</sup>) of Cd–O···O (multiple scattering paths) were defined as 3<sup>\*</sup> $\sigma^2$  (Å<sup>2</sup>) for the Cd–O paths.

probably, the involvement of Fe and Al in the second shell was relatively more likely than in most of the other samples.

### 3.2. Batch experiments and modelling

Sorption of cadmium(II), copper(II) and lead(II) was weakest at low pH, as could be expected (Fig. 1, Fig. S6 and Fig. 2). For copper(II) and lead(II) the sorption decreased again at high pH, likely because of dissolution of NOM-organic complexes (Gustafsson et al., 2003). Generally, there were no or small effects on metal sorption after the addition of PO<sub>4</sub>–P (Fig. S5), implying that a P-related enhancement of metal sorption did not occur to any great extent.

The modelling with Visual MINTEQ was performed in steps. First, default parameters were used for  $f_{HS}$  and for the SSA of ferrihydrite (0.55 and 650 m<sup>2</sup> g<sup>-1</sup>, respectively). Under these conditions NOM complexes dominated for cadmium(II) and copper(II), whereas for lead(II) ferrihydrite was important. For all soils except Romfartuna Bhs the modelled adsorption edges were displaced to the left of the observations, showing that the default parameters overestimated sorption (Fig. 1 and Fig. S6). We investigated

whether an improved description could be made with a decreased  $f_{HS}$  value, reflecting an ‘inactivation’ of soil HA and FA as a result of their coordination onto Fe and Al (hydr)oxides including allophane (Gustafsson et al., 2003). This was done for cadmium(II) and copper(II) as the binding to HA and FA dominated for these metals, and was carried out by trial-and-error until the model described the adsorption edges for both copper(II) and cadmium(II) well (Fig. 1, Fig. S6, right column). The optimised  $f_{HS}$  values ranged from 0.062 to 0.25 for different soils (Table 4).

Still however, the model with the adjusted  $f_{HS}$  values was not able to describe lead(II) sorption, which was still strongly overestimated (again with the exception for Romfartuna Bhs; see Fig. 2, left column). Moreover, under these conditions ferrihydrite was the dominant sorbent for Kloten 2 Bs, which was not in agreement with the EXAFS results. It was therefore concluded that the used model setup resulted in too strong lead(II) adsorption to the soil ferrihydrite, except in the case of Romfartuna Bhs. To deal with this, a number of approaches was tested. Of these, two were successful in simulating the observed lead(II) adsorption. First, it was assumed that the specific surface area (SSA) was too high, and that this

**Table 3**Summary of shell fit results: lead(II) L<sub>3</sub>-edge EXAFS of soil samples and standards. Parameters in italics were constrained during fitting.

Sample	Path	CN	R (Å)	$\sigma^2$ (Å <sup>2</sup> )	$\Delta E$ (eV)	$S_0^2$	R-factor (%)
Kloten Pb low 2.3 mmol kg <sup>-1</sup> Pb pH 5.40	Pb–O1	2.0 (0.2)	2.32 (0.01)	0.012 (0.002)	–10.9 (0.9)	1	0.6
	Pb···O/C2	1.1 (0.2)	3.08 (0.21)	<i>0.01</i>			
k-range 2.3–8							
Kloten Pb+P low 2.3 mmol kg <sup>-1</sup> Pb 11.4 mmol kg <sup>-1</sup> P pH 5.19	Pb–O1	2.1 (0.5)	2.34 (0.03)	0.011 (0.004)	–10.6 (1.7)	1	0.8
	Pb···O/C2	1.3 (0.5)	3.07 (0.04)	<i>0.01</i>			
k-range 2.3–7.2							
Kloten Pb+As low 2.3 mmol kg <sup>-1</sup> Pb 11.4 mmol kg <sup>-1</sup> As(V) pH 5.40	Pb–O1	3.1 (0.4)	2.37 (0.01)	0.022 (0.002)	–8.4 (1.0)	1	0.6
	Pb···O/C2	0.5 (0.2)	3.12 (0.04)	<i>0.01</i>			
k-range 2.3–8							
Kloten Pb high 4.5 mmol kg <sup>-1</sup> Pb pH 4.91	Pb–O1	2.3 (0.3)	2.34 (0.01)	0.014 (0.003)	–10.4 (0.9)	1	0.9
	Pb···O/C2	1.0 (0.3)	3.09 (0.03)	<i>0.01</i>			
k-range 2.3–8							
Kloten Pb+P high 4.5 mmol kg <sup>-1</sup> Pb 11.4 mmol kg <sup>-1</sup> P pH 4.89	Pb–O1	2.9 (0.3)	2.36 (0.01)	0.019 (0.002)	–10.1 (0.7)	1	0.4
	Pb···O/C2	0.8 (0.2)	3.09 (0.03)	<i>0.01</i>			
k-range 2.3–8							
Pb-FA 3 mM Pb, 8 g L <sup>-1</sup> FA pH 5.75	Pb–O1	3.9 (0.4)	2.37 (0.01) (0.006)	0.021 (0.002)	–8.8 (0.9)	1	0.5
	Pb···C	2	3.23 (0.04)	0.019 (0.006)			
k-range 2.3–8							
Pb-Fh 30 μM Pb <sup>2+</sup> 0.3 mM Fe pH 5.16	Pb–O1	2	2.36 (0.03)	0.011 (0.003)	–1.1 (2.5)	1	4.2
	Pb–O2	4	2.62 (0.04)	0.026 (0.008)			
	Pb···Fe	1	3.40 (0.04)	0.013 (0.005)			
k-range 2.3–9							
Pb–P-Fh 30 μM Pb <sup>2+</sup> , 60 μM P 0.3 mM Fe pH 4.68	Pb–O1	2	2.33 (0.05)	0.011 (0.004)	–8.1 (3.2)	1	1.5
	Pb–O2	4	2.56 (0.07)	0.006 (0.008)			
	Pb···Fe1	0.4 (0.4)	3.36 (0.10)	<i>0.013</i>			
	Pb···Fe2	0.6	4.03 (0.10)	0.010 (0.020)			
k-range 2.25–8							
Pb-Alox 50 μM Pb <sup>2+</sup> 1 mM Al pH 5.92	Pb–O1	2	2.28 (0.02)	0.007 (0.003)	–5.7 (1.5)	1	1.1
	Pb···Al	1	3.34 (0.05)	0.019 (0.009)			
k-range 2.25–8							

CN = Coordination number; R = Atomic distance;  $\sigma^2$  = Debye-Waller factor;  $\Delta E$  = Energy shift parameter;  $S_0^2$  = Passive amplitude reduction factor; R = R-factor = Athena goodness-of-fit parameter. Uncertainties of fitted parameters as given in Artemis (Ravel and Newville, 2005).

Added concentrations of lead(II), phosphate and arsenate are listed below the sample name.

parameter could be adjusted for individual Bs horizons. This resulted in very good fits (not shown), but the adjusted SSA:s of the Kloten and Risbergshöjden samples were as low as 100 m<sup>2</sup> g<sup>-1</sup>, implying a low reactivity of the accumulated ferrihydrite. However, this does not agree with other observations for Kloten 1 Bs2 and for similar soils, showing that the adsorption of SO<sub>4</sub><sup>2-</sup> and As(V) was strong, which required a relatively high SSA in the anion adsorption model (Gustafsson, 2006). Therefore the second option, which also resulted in very good fits, was chosen for further study: the adjustment of PZC to higher values to reflect the spillover effect from allophane, as explained above.

Thus, in the second step of the modelling the PZC(Fh) was increased until the modelled lead(II) adsorption edges were in agreement with the observations. The optimised PZC:s ranged from 8.1 to 9.1 (Table 4). The model was now able to describe also lead(II) sorption well (Fig. 2, right column). The final model indicated that for cadmium(II) and copper(II), the sorption was dominated by complexation to NOM, whereas for lead(II) most of the sorption was governed by NOM, although ferrihydrite was partly responsible for sorption (example shown in Fig. S7). Hence the final model, with its adjusted  $f_{HS}$  and PZC(Fh) values, agreed (at least in a qualitative sense) with the EXAFS results for both cadmium(II) and lead(II).

Finally, the model was applied to investigate whether it could mimic the results of the batch experiment with added PO<sub>4</sub>-P. For cadmium(II) and copper(II) no effects of P were seen (data not

shown), which was expected given the near complete dominance of NOM complexes both according to the EXAFS results (for cadmium) and to the modelling. However, also for lead(II), for which sorption to ferrihydrite was more important, the model only predicted a very modest enhancement of lead(II) sorption similar to observations (Fig. 3). Why, then, was PO<sub>4</sub>-P found to have a much smaller effect on lead(II) sorption in this study compared to the ferrihydrite systems of Tiberg et al. (2013)? A detailed interpretation of the model result highlighted the following three factors as being of importance: (i) a large part of the sorbed lead(II) was bound to NOM, not to ferrihydrite; (ii) the equilibrium concentration of PO<sub>4</sub>-P was much lower in the current study than in the one of Tiberg et al. (2013), and (iii) the presence of initially adsorbed SO<sub>4</sub>, which had decreased the net (positive) surface charge of the ferrihydrite. This limited the electrostatic effect of the added PO<sub>4</sub> ions, and at the same time the adsorbed SO<sub>4</sub> favoured formation of the bidentate (FeOH)<sub>2</sub>Pb<sup>+</sup> complex relative to the ternary surface complex (FeO)<sub>2</sub>HPPbO<sub>3</sub>H<sup>0</sup>.

### 3.3. Possible reasons for the low reactivity of organic matter and ferrihydrite

The low optimised values of  $f_{HS}$  and PZC of ferrihydrite show that default model parameters, derived for soil surface horizons, cannot be used to predict metal sorption in many Bs horizons.

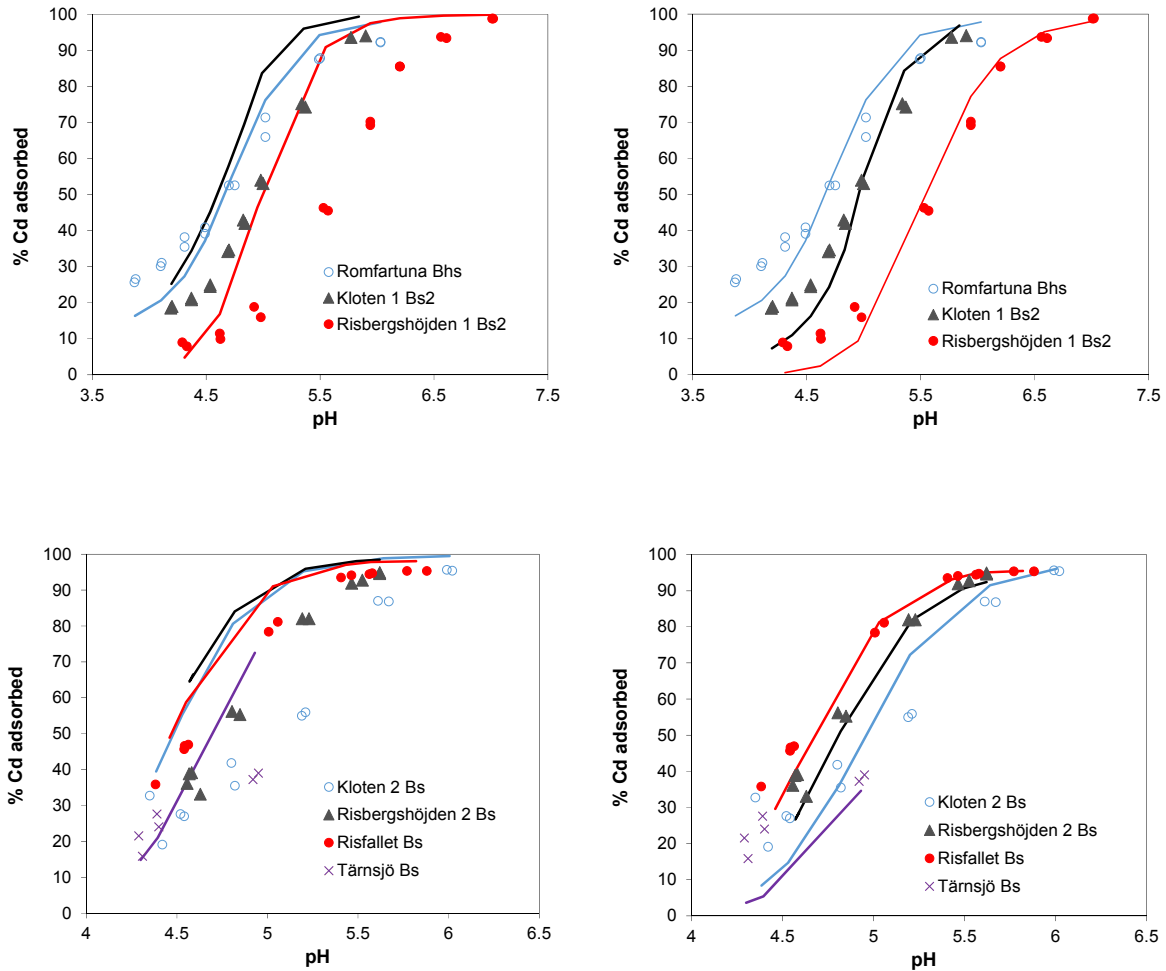


**Fig. 1.** Cadmium(II) adsorption as a function of pH. Points are observations and lines are model fits. Left column: Model fits assuming default parameters, i.e.  $f_{HS} = 0.55$  and  $PZC(Fh) = 8.1$ . Right column: Model fits with adjusted parameters (see Table 4).

There appears to be a relationship between  $f_{HS}$  and the ratio of pyrophosphate-to oxalate-extractable Al (Table 4 and Fig. S8). At low ratios, the  $f_{HS}$  values are very small, whereas when the  $Al_{pypp}/Al_{ox}$  ratio is high, as for Romfartuna Bhs,  $f_{HS}$  is in better accordance with default parameters. The low  $f_{HS}$  values in soils with low  $Al_{pypp}/Al_{ox}$  ratios may be explained by strong sorption of the NOM carboxylate groups to Fe and Al (hydr)oxide surfaces, reducing the number of available carboxylate groups. This leads to a negative deviation from additivity, as shown for the Cd-HA-hematite system under low-pH conditions (Vermeer et al., 1999). Possibly the relationship to the  $Al_{pypp}/Al_{ox}$  ratio may be used to predict the  $f_{HS}$  value for a given Bs horizon, but additional data from other Bs horizons are required for confirmation.

Moreover, the model results suggest that the observed lack of importance of ferrihydrite for lead(II) sorption may in part be due to surface charge effects from allophane, which made lead(II) adsorption thermodynamically less favourable as compared to freshly precipitated, “pure” ferrihydrite. The amounts of ferrihydrite and allophane can be estimated from their oxalate- and pyrophosphate concentrations, i.e. from  $Fe_{ox}$  and  $Al_{ox} - Al_{pypp}$ , respectively (Gustafsson, 2001). In Bs horizons in which the amount of ferrihydrite was much smaller than that of allophane (as reflected in the  $Fe_{ox}/(Fe_{ox} + Al_{ox} - Al_{pypp})$  ratio), the optimised

$PZC(Fh)$  tended to be higher (Fig. S9), in line with this reasoning. Such an effect has not been previously documented, but may be a contributing factor behind why Spodosol Bs horizons with low  $Fe_{ox}/(Fe_{ox} + Al_{ox} - Al_{pypp})$  ratios exhibit strong anion adsorption and weak  $Pb^{2+}$  adsorption characteristics at the same time (compare with Gustafsson, 2006). This does not exclude the presence of other effects that may cause a low reactivity of the precipitated ferrihydrite in these horizons. For example, a low DOC concentration may enhance the crystallisation of 2-line ferrihydrite to 6-line ferrihydrite and to other Fe oxides (e.g. Eusterhues et al., 2008) with lower surface areas. In theory, it is possible to explain the observed results if one assumes that the accumulated ferrihydrite and allophane have a low and high SSA, respectively, causing a low lead(II) adsorption to the former and a strong anion adsorption to the latter. However, this seems to be at odds with the observed intergrowth between the two phases (as indicated by Karlton et al., 2000), and also with the observation that adsorbed vanadate was equally distributed between ferrihydrite and an  $Al(OH)_3$ -type phase (possibly allophane) in Risbergshöjden 2 Bs (Larsson et al., 2017). For these reasons, we hypothesize that it is the surface charge effect of co-accumulated allophane that is the main reason for the unexpectedly low lead(II) adsorption in Bs horizons with a low ratio of accumulated Fe to Al.

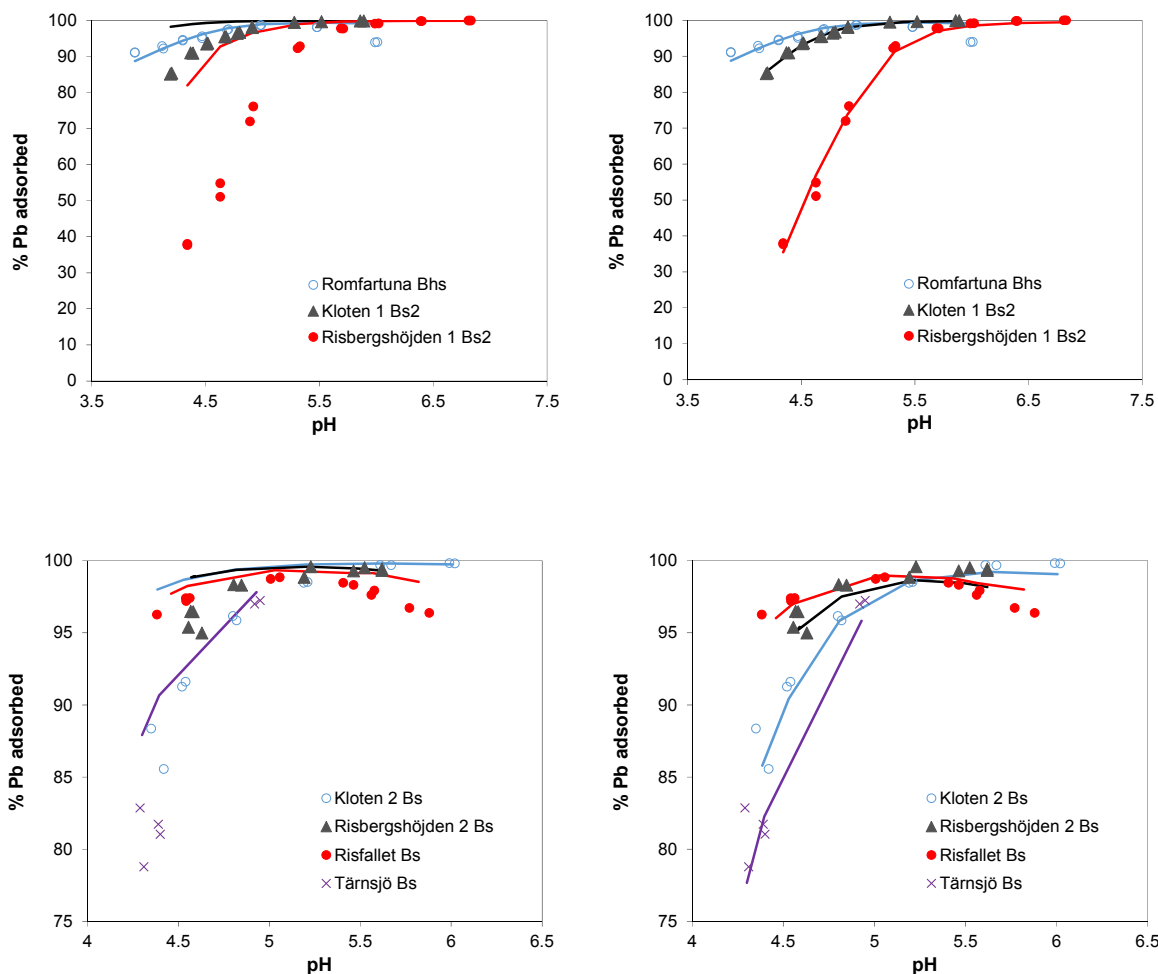


**Fig. 2.** Lead(II) adsorption as a function of pH. Points are observations and lines are model fits. Left column: Model fits using the optimised  $f_{HS}$  from the cadmium and copper systems, but with the default  $PZC(Fh) = 8.1$ . Right column: Model fits with adjusted  $PZC(Fh)$  values (see Table 4).

**Table 4**

Default and optimised values of the fraction active organic matter ( $f_{HS}$ ), the point-of zero charge (PZC) of ferrihydrite (Fh) as used in the SHM and CD-MUSIC models, and the  $Al_{pyp}/Al_{ox}$  ratio.

Sample	$f_{HS}$ (Default)	$f_{HS}$ (Optimised)	PZC of Fh (Default)	PZC of Fh (Optimised)	$Al_{pyp}/Al_{ox}$
Klotten 1 Bs2	0.55	0.13	8.1	9.1	0.442
Klotten 2 Bs	"	0.089	"	9.0	0.436
Risbergshöjden 1 Bs2	"	0.062	"	8.9	0.083
Risbergshöjden 2 Bs	"	0.12	"	8.8	0.328
Risfallet Bs	"	0.25	"	8.4	0.636
Romfartuna Bhs	"	0.55	"	8.1	0.728
Tärsjö Bs	"	0.13	"	8.4	0.551

#### 4. Conclusions

Cadmium(II) and copper(II) adsorption to seven Spodosol Bs horizons was governed by organic matter complexation, whereas for lead(II) both organic matter complexation and Fe/Al (hydr)oxide sorption may be involved, although the former predominated according to the EXAFS results for the Klotten 2 Bs sample. For cadmium(II) carboxylate groups were the most significant complexing ligands. Addition of phosphate or arsenate to  $1 \mu\text{mol L}^{-1}$  did not result in any major shifts in metal speciation, and did not enhance the adsorption of any of the three metals to any significant extent.

An assemblage model with default parameters derived for soil surface horizons overestimated metal sorption in six out of seven Bs horizons. To provide model fits in accordance with the experimental results, substantial decreases of the fraction active organic matter were necessary, and the PZC of ferrihydrite had to be increased. The final model indicates that in Spodosol Bs horizons with low  $Al_{pyp}/Al_{ox}$  ratios, humic and fulvic acids are less accessible for metal sorption through their interaction with Fe and Al (hydr) oxides. At the same time the reactivity of ferrihydrite is low, possibly because of spillover of positive surface potential from allophane components.

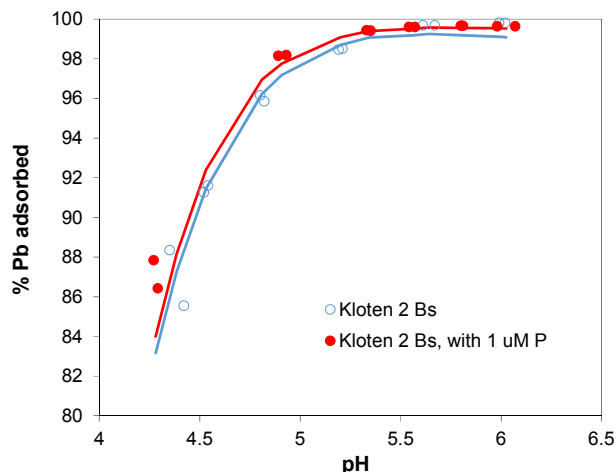


Fig. 3. Lead adsorption as a function of pH for the Klotten 2 Bs soil, with and without the presence of  $1 \mu\text{mol L}^{-1} \text{PO}_4\text{-P}$  in the equilibrium solution. Points are observations and lines are model fits.

## Acknowledgments

The study was funded by the Geological Survey of Sweden. This work was carried out with the support of the Diamond Light Source (experiment SP8188). The support from Andy Dent at beamline B18 is gratefully acknowledged. Use of the National Synchrotron Light Source, Brookhaven National Laboratory, was supported by the U.S. Department of Energy, Office of Science, Office of Basic Energy Sciences, under Contract No. DE-AC02-98CH10886. Use of the Stanford Synchrotron Radiation Lightsource, SLAC National Accelerator Laboratory, is supported by the U.S. Department of Energy, Office of Science, Office of Basic Energy Sciences under Contract No. DE-AC02-76SF00515.

## Appendix B. Supplementary data

Supplementary data related to this article can be found at <https://doi.org/10.1016/j.chemosphere.2018.01.004>.

## References

- Cancès, B., Ponthieu, M., Castrec-Rouelle, M., Aubry, E., Benedetti, M.F., 2003. Metal ions speciation in soil and its solution: experimental data and model results. *Geoderma* 113, 341–355. [https://doi.org/10.1016/S0016-7061\(02\)00369-5](https://doi.org/10.1016/S0016-7061(02)00369-5).
- Chukalina, M., 2010. Wavelet2.ipf, a Procedure for Calculating the Wavelet Transform in IGOR Pro. Grenoble, France, 2010.
- Davis, J.A., Coston, J.A., Kent, D.B., Fuller, C.C., 1998. Application of the surface complexation concept to complex mineral assemblages. *Environ. Sci. Technol.* 32, 2820–2828. <https://doi.org/10.1021/es980312q>.
- Dzombak, D.A., Morel, F.M.M., 1990. *Surface Complexation Modeling*. Wiley & Sons, New York.
- Eusterhues, K., Wagner, F.E., Häusler, W., Hanzlik, M., Knicker, H., Totsche, K.U., Kögel-Knabner, I., Schwertmann, U., 2008. Characterization of ferrihydrite-soil organic matter coprecipitates by X-ray diffraction and Mössbauer spectroscopy. *Environ. Sci. Technol.* 42, 7891–7897. <https://doi.org/10.1021/es800881w>.
- Flogeac, K., Guillon, E., Aplincourt, M., 2004. Surface complexation of copper(II) on soil particles: EPR and XAFS studies. *Environ. Sci. Technol.* 38, 3098–3103. <https://doi.org/10.1021/es049973f>.
- Fulda, B., Voegelin, A., Kretzschmar, R., 2013. Redox-controlled changes in cadmium solubility and solid-phase speciation in a paddy soil as affected by reducible sulfate and copper. *Environ. Sci. Technol.* 47, 12775–12783. <https://doi.org/10.1021/es401997d>.
- Funke, H., Scheinost, A., Chukalina, M., 2005. Wavelet analysis of extended X-ray absorption fine structure data. *Phys. Rev. B* 71, 094110. <https://doi.org/10.1103/PhysRevB.71.094110>.
- Groenenberg, J.E., Lofts, S., 2014. The use of assemblage models to describe trace element partitioning, speciation, and fate: a review. *Environ. Toxicol. Chem.* 33, 2181–2196. <https://doi.org/10.1002/etc.2642>.
- Gustafsson, J.P., 2001. Modeling the acid-base properties and metal complexation of

- humic substances with the Stockholm Humic Model. *J. Colloid Interface Sci.* 244, 102–112. <https://doi.org/10.1006/jcis.2001.7871>.
- Gustafsson, J.P., 2006. Arsenate adsorption to soils: modelling the competition from humic substances. *Geoderma* 135, 320–330. <https://doi.org/10.1016/j.geoderma.2006.03.046>.
- Gustafsson, J.P., Berggren, D., Simonsson, M., Zysset, M., Mulder, J., 2001. Aluminium solubility mechanisms in moderately acid Bs horizons of podzolised soils. *Eur. J. Soil Sci.* 52, 655–665. <https://doi.org/10.1046/j.1365-2389.2001.00400.x>.
- Gustafsson, J.P., Kleja, D.B., 2005. Modeling salt-dependent proton binding by organic soils with the NICA-Donnan and with the Stockholm Humic models. *Environ. Sci. Technol.* 39, 5372–5377. <https://doi.org/10.1021/es050332z>.
- Gustafsson, J.P., Pechova, P., Berggren, D., 2003. Modeling metal binding to soils: the role of natural organic matter. *Environ. Sci. Technol.* 37, 2767–2774. <https://doi.org/10.1021/es026249t>.
- Gustafsson, J.P., Tiberg, C., Edkymish, A., Kleja, D.B., 2011. Modelling lead(II) sorption to ferrihydrite and soil organic matter. *Environ. Chem.* 8, 485–492. <https://doi.org/10.1071/EN11025>.
- Gustafsson, J.P., Akram, M., Tiberg, C., 2015. Predicting sulphate adsorption/desorption in forest soils: evaluation of an extended Freundlich equation. *Chemosphere* 119, 83–89. <https://doi.org/10.1016/j.chemosphere.2014.05.067>.
- Gustafsson, J.P., 2016. Visual MINTEQ version 3.1. Available from: <https://vminteq.lwr.kth.se>. (Accessed 5 January 2018).
- Hiemstra, T., 2013. Surface and mineral structure of ferrihydrite. *Geochim. Cosmochim. Acta* 105, 316–325. <https://doi.org/10.1016/j.gca.2012.12.002>.
- Hiemstra, T., van Riemsdijk, W.H., 1996. A surface structural approach to ion adsorption: the charge distribution (CD) model. *J. Colloid Interface Sci.* 179, 488–508. <https://doi.org/10.1006/jcis.1996.0242>.
- Karlsson, T., Persson, P., Skyllberg, U., 2005. Extended X-ray absorption fine structure spectroscopy evidence for the complexation of cadmium by reduced sulfur groups in natural organic matter. *Environ. Sci. Technol.* 39, 3048–3055. <https://doi.org/10.1021/es048585a>.
- Karlton, E., Bain, D.C., Gustafsson, J.P., Mannerkoski, H., Murad, E., Wagner, U., 2000. Surface reactivity of poorly ordered minerals in podzol B horizons. *Geoderma* 94, 265–288. [https://doi.org/10.1016/S0016-7061\(98\)00141-4](https://doi.org/10.1016/S0016-7061(98)00141-4).
- Kelly, S.D., Hesterberg, D., Ravel, B., 2008. Analysis of soils and minerals using X-ray absorption spectroscopy. In: Ulery, A.L., Drees, L.R. (Eds.), *Methods of Soil Analysis. Part 5. Mineralogical Methods*. Soil Science of America, Madison, WI, USA, pp. 387–463. *Soil Science of America Book Series No. 5*.
- Kinniburgh, D.G., van Riemsdijk, W.H., Koopal, L.K., Borkovec, M., Benedetti, M.F., Avena, M.F., 1999. Ion binding to natural organic matter: heterogeneity, stoichiometry, and thermodynamic consistency. *Colloid. Surface. A* 151, 147–166. [https://doi.org/10.1016/S0927-7757\(98\)00637-2](https://doi.org/10.1016/S0927-7757(98)00637-2).
- Larsson, M.A., Hadialhejazi, G., Gustafsson, J.P., 2017. Vanadium sorption by mineral soils: development of a predictive model. *Chemosphere* 168, 925–932. <https://doi.org/10.1016/j.chemosphere.2016.10.117>.
- Liu, X., Millero, F.J., 1999. The solubility of iron hydroxide in sodium chloride solutions. *Geochim. Cosmochim. Acta* 63, 3487–3497. [https://doi.org/10.1016/S0016-7037\(99\)00270-7](https://doi.org/10.1016/S0016-7037(99)00270-7).
- Lofts, S., Tipping, E., 2000. Solid-solution metal partitioning in the Humber rivers: application of WHAM and SCAMP. *Sci. Total Environ.* 251–252, 381–390. [https://doi.org/10.1016/S0048-9697\(00\)00418-6](https://doi.org/10.1016/S0048-9697(00)00418-6).
- Lumsdon, D.G., 1996. Modelling cadmium retention by soils and the effects of aluminium competition. *Appl. Geochem.* 11, 285–291. [https://doi.org/10.1016/0883-2927\(95\)00048-8](https://doi.org/10.1016/0883-2927(95)00048-8).
- Lumsdon, D.G., 2004. Partitioning of organic carbon, aluminium, and cadmium between solid and solution in soils: application of a mineral-humic particle additivity model. *Eur. J. Soil Sci.* 55, 271–285. <https://doi.org/10.1111/j.1365-2389.2004.00599.x>.
- Martínez-Villegas, N., Martínez, C.E., 2008. Solid- and solution phase organics dictate copper distribution and speciation in multicomponent systems containing ferrihydrite, organic matter, and montmorillonite. *Environ. Sci. Technol.* 42, 2833–2838. <https://doi.org/10.1021/es072012r>.
- Morin, G., Oostergren, J.D., Juillot, F., Ildefonse, P., Calas, G., Brown, G.E., 1999. XAFS determination of the chemical form of lead in smelter-contaminated soils and mine tailings: importance of adsorption process. *Am. Miner.* 84, 420–434. <https://doi.org/10.2138/am-1999-0327>.
- Rate, A.W., 2010. Sorption of cadmium(II) and copper(II) by soil humic acids: temperature effects and sorption heterogeneity. *Chem. Ecol.* 5, 371–383. <https://doi.org/10.1080/02757540.2010.504666>.
- Ravel, B., Newville, M., 2005. Athena Artemis Hephaestus: data analysis for X-ray absorption spectroscopy using IFEFFIT. *J. Synchrotron Radiat.* 12, 537–541. <https://doi.org/10.1107/S0909049505012719>.
- Scheffel, K.G., Ryan, J.A., 2004. Spectroscopic speciation and quantification of lead in phosphate-amended soils. *J. Environ. Qual.* 33, 1288–1295. <https://doi.org/10.2134/jeq2004.1288>.
- Shi, Z., Allen, H.E., Di Toro, D.M., Lee, S.-Z., Meza, D.M.F., Lofts, S., 2007. Predicting cadmium adsorption on soils using WHAM VI. *Chemosphere* 69, 605–612. <https://doi.org/10.1016/j.chemosphere.2007.03.001>.
- Shi, Z., Allen, H.E., Di Toro, D.M., Lee, S.-Z., Harsh, J.B., 2013. Predicting Pb<sup>II</sup> adsorption on soils: the roles of organic matter, cation competition and iron (hydr)oxides. *Environ. Chem.* 10, 465–474. <https://doi.org/10.1071/EN13153>.
- Strawn, D.G., Sparks, D.L., 2001. Effects of soil organic matter on the kinetics and mechanisms of lead(II) sorption and desorption in soil. *Soil Sci. Soc. Am. J.* 64, 144–156. <https://doi.org/10.2136/sssaj2000.641144x>.
- Soil Survey Staff, 2014. *Keys to Soil Taxonomy*, twelfth ed. National Resources

- Conservation Service, United States Department of Agriculture, Washington DC.
- Tiberg, C., Gustafsson, J.P., 2016. Phosphate effects on cadmium(II) sorption to ferrihydrite. *J. Colloid Interface Sci.* 471, 103–111. <https://doi.org/10.1016/j.jcis.2016.03.016>.
- Tiberg, C., Sjöstedt, C., Persson, I., Gustafsson, J.P., 2013. Phosphate effects on copper(II) and lead(II) sorption to ferrihydrite. *Geochim. Cosmochim. Acta* 120, 140–157. <https://doi.org/10.1016/j.gca.2013.06.012>.
- Tipping, E., 2002. *Cation Binding by Humic Substances*. Cambridge University Press, Cambridge, UK.
- Tipping, E., Lofts, S., Sonke, J.E., 2011. Humic ion binding model VII: a revised parameterisation of cation-binding by humic substances. *Environ. Chem.* 8, 225–235. <https://doi.org/10.1071/EN11016>.
- van Reeuwijk, L.P., 1995. *Procedures for Soil Analyses*, fifth ed. International Soil Reference and Information Centre, Wageningen, Netherlands.
- Vermeer, A.W.P., McCulloch, J.K., van Riemsdijk, W.H., Koopal, L.K., 1999. Metal ion adsorption to complexes of humic acids and metal oxides: deviations from the additivity rule. *Environ. Sci. Technol.* 33, 3892–3897. <https://doi.org/10.1021/es990260k>.
- Weng, L.P., Temminghoff, E.J.M., van Riemsdijk, W.H., 2001. Contribution of individual sorbents to the control of heavy metal activity in sandy soil. *Environ. Sci. Technol.* 32, 4436–4443. <https://doi.org/10.1021/es010085j>.
- Weng, L.P., Temminghoff, E.J.M., Lofts, S., Tipping, E., van Riemsdijk, W.H., 2002. Complexation with dissolved organic matter and solubility control of heavy metals in a sandy soil. *Environ. Sci. Technol.* 36, 4804–4810. <https://doi.org/10.1021/es0200084>.
- Xia, K., Bleam, W.F., Helmke, P.A., 1997. Studies of the nature of Cu<sup>2+</sup> and Pb<sup>2+</sup> binding sites in soil humic substances using X-ray absorption spectroscopy. *Geochim. Cosmochim. Acta* 61, 2211–2221. [https://doi.org/10.1016/S0016-7037\(97\)00079-3](https://doi.org/10.1016/S0016-7037(97)00079-3).
- Xiong, J., Koopal, L.K., Tan, W.F., Fang, L.C., Wang, M.X., Zhao, W., Liu, F., Zhang, J., Weng, L., 2013. Lead binding to soil fulvic and humic acids: NICA-Donnan modeling and XAFS spectroscopy. *Environ. Sci. Technol.* 47, 11634–11642. <https://doi.org/10.1021/es402123v>.
- Zabinsky, S.I., Rehr, J.J., Ankudinov, A., Albers, R.C., Eller, M.J., 1995. Multiple-scattering calculations of x-ray-absorption spectra. *Phys. Rev. B* 52, 2995–3009. <https://doi.org/10.1103/PhysRevB.52.2995>.

*Supplementary material for:*

## **Metal sorption to Spodosol Bs horizons: organic matter complexes predominate**

Charlotta Tiberg<sup>a,b</sup>, Carin Sjöstedt<sup>a</sup>, Jon Petter Gustafsson<sup>a,c,\*</sup>

<sup>a</sup> Department of Soil and Environment, Swedish University of Agricultural Sciences, Box 7014, SE-750 07 Uppsala, Sweden

<sup>b</sup> Present Address: Swedish Geotechnical Institute, Kornhamnstorg 61, SE-111 27 Stockholm, Sweden

<sup>c</sup> Department of Sustainable Development, Environmental Science and Engineering, KTH Royal Institute of Technology, Teknikringen 10B, SE-100 44 Stockholm, Sweden

Number of pages: 11

Number of tables: 3

Number of figures: 9

### **Contents:**

	page
Table S1. Concentrations of metals and phosphate added to the soil suspensions	2
Table S2. Geochemically active metals as estimated by extraction	2
Table S3. Parameter values for cation complexation in the SHM	3
Table S4. Surface complexation reactions in the CD-MUSIC model for ferrihydrite	4
Fig. S1. Cadmium K-edge EXAFS spectra	5
Fig. S2. Wavelet transforms of Cd K edge EXAFS spectra for the Kloten samples	6
Fig. S3. Fourier Transforms (Real part) of Cd K-edge EXAFS spectra	6
Fig. S4. Lead L <sub>3</sub> -edge EXAFS spectra	7
Fig. S5. Percent Cu, Cd and Pb sorbed as a function of pH as influenced by P	8
Fig. S6. Copper adsorption as a function of pH. Observations and model fits	9
Fig. S7. Modelled contributions of Cd, Cu and Pb bound to ferrihydrite and organic matter	10
Fig. S8. The $f_{HS}$ value as a function of the $Al_{ox}/Al_{py}$ ratio	10
Fig. S9. Optimized PZC of soil ferrihydrite as the fraction of poorly crystalline Fe oxide	11
References	11

**Table S1**Concentrations of metals and phosphate added to the B horizon soil suspensions<sup>a</sup>

Soil	Cd <sup>2+</sup>	Cu <sup>2+</sup>	Pb <sup>2+</sup>	PO <sub>4</sub> -P <sup>b</sup>
	mmol kg <sup>-1</sup>			
Kloten 1 Bs2	0.31	-	0.79	-
Kloten 2 Bs	0.068	0.68	0.68	11.4
Risbergshöjden 1 Bs2	0.33	1.64	1.64	-
Risbergshöjden 2 Bs	0.056	0.56	0.56	9.3
Risfallet Bs	0.058	0.58	0.58	4.8
Romfartuna Bhs	0.17	-	0.34	-
Tärnsjö Bs	0.038	0.38	0.38	0.48

<sup>a</sup>For the Kloten 2, Risbergshöjden 2, Risfallet and Tärnsjö soils all metals (Cd<sup>2+</sup>, Cu<sup>2+</sup> and Pb<sup>2+</sup>) were added together, whereas in the other soils the metals were added individually in separate experiments.

<sup>b</sup>In one set of experiments, PO<sub>4</sub>-P was not added, whereas in the second set, PO<sub>4</sub>-P was added with the concentration shown here to give an equilibrium concentration of around 1 µM dissolved P.

**Table S2**

Geochemically active metals, as estimated by extraction

Soil	Cd <sup>2+</sup>	Cu <sup>2+</sup>	Pb <sup>2+</sup>
	µmol kg <sup>-1</sup>		
Kloten 1 Bs2	0.3	-	13
Kloten 2 Bs	0.1	44	26
Risbergshöjden 1 Bs2	0.1	40	4
Risbergshöjden 2 Bs	0.1	18	50
Risfallet Bs	0.4	36	52
Romfartuna Bhs	0.2	-	11
Tärnsjö Bs	0.1	12	14

For the Kloten 2, Risbergshöjden 2, Risfallet and Tärnsjö soils, 2 g soil was shaken with 35 cm<sup>3</sup> 0.1 M HNO<sub>3</sub> for 16 h (Gustafsson and Kleja, 2005). The filtered supernatants were analysed for Cd, Cu and Pb by ICP-OES.

For the Kloten 1, Risbergshöjden 1, and Romfartuna soils, the above results were originally published by Gustafsson et al. (2003). 3 g soil was shaken with 30 cm<sup>3</sup> 0.5 M NH<sub>4</sub>OAc/0.016 M EDTA solution at pH 4.65 for 2 h. The filtered supernatants were analysed for Cd, Cu and Pb by GFAAS.

**Table S3**

Parameter values for cation complexation to soil organic matter in the Stockholm Humic Model (SHM)<sup>a</sup>

Cation	Humic acid and fulvic acid			
	$\log K_{Mm}$	$\log K_{Mb}$	$\log K_{MbOH}$	$\Delta LK_2$
Al <sup>3+</sup>	-	-4.06	-9.45	1.05
Ca <sup>2+</sup>	-2.2	-	-	0.3
Fe <sup>3+</sup>	-	-1.68	-4.6	1.7
Mg <sup>2+</sup>	-2.5	-	-	0.3
Cd <sup>2+</sup>	-1.6	-9.5	-	1.3
Cu <sup>2+</sup>	-0.55	-6.0	-13.6	1.4
Pb <sup>2+</sup>	-0.40	-5.92	-	0.98 / 1.55 <sup>b</sup>
High-affinity ligand				
	$\log K_{Mm}$	Site concentration		
Pb <sup>2+</sup>	3.0	0.01 % of organic C content		

<sup>a</sup>The constants are the same as used in earlier publications (e.g. Linde et al. 2007; Gustafsson et al. 2011). However, the method to calculate the site concentration of the high-affinity ligand for Pb<sup>2+</sup> was revised in this study, see text.

<sup>b</sup>The  $\Delta LK_2$  value for the  $\log K_{Mm}$  constant of solid-phase organic matter was set to 1.55; for the  $\log K_{Mb}$  constant of solid-phase organic matter, and for the constants for dissolved organic matter,  $\Delta LK_2 = 0.98$ .

**Table S4**Surface complexation reactions and constants used in the CD-MUSIC model for ferrihydrite<sup>a</sup>.

Reaction	$(\Delta z_0, \Delta z_1, \Delta z_2)^b$	$\log K^c$
$\text{FeOH}^{1/2-} + \text{H}^+ \leftrightarrow \text{FeOH}_2^{1/2+}$	(1,0,0)	8.1 <sup>d</sup>
$\text{Fe}_3\text{O}^{1/2-} + \text{H}^+ \leftrightarrow \text{Fe}_3\text{OH}^{1/2+}$	(1,0,0)	8.1 <sup>d</sup>
$\text{FeOH}^{1/2-} + \text{Na}^+ \leftrightarrow \text{FeOHNa}^{1/2+}$	(0,1,0)	-0.6
$\text{Fe}_3\text{O}^{1/2-} + \text{Na}^+ \leftrightarrow \text{Fe}_3\text{ONa}^{1/2+}$	(0,1,0)	-0.6
$\text{FeOH}^{1/2-} + \text{H}^+ + \text{NO}_3^- \leftrightarrow \text{FeOH}_2\text{NO}_3^{1/2-}$	(1,-1,0)	7.42 <sup>d</sup>
$\text{Fe}_3\text{O}^{1/2-} + \text{H}^+ + \text{NO}_3^- \leftrightarrow \text{Fe}_3\text{OHNO}_3^{1/2-}$	(1,-1,0)	7.42 <sup>d</sup>
$2\text{FeOH}^{1/2-} + 2\text{H}^+ + \text{PO}_4^{3-} \leftrightarrow \text{Fe}_2\text{O}_2\text{PO}_2^{2-} + 2\text{H}_2\text{O}$	(0.46,-1.46,0)	27.59
$2\text{FeOH}^{1/2-} + 3\text{H}^+ + \text{PO}_4^{3-} \leftrightarrow \text{Fe}_2\text{O}_2\text{POOH}^- + 2\text{H}_2\text{O}$	(0.63,-0.63,0)	32.89
$\text{FeOH}^{1/2-} + 3\text{H}^+ + \text{PO}_4^{3-} \leftrightarrow \text{FeOPO}_3\text{H}_2^{1/2-} + \text{H}_2\text{O}$	(0.5,-0.5,0)	30.23
$\text{FeOH}^{1/2-} + \text{H}^+ + \text{SO}_4^{2-} \leftrightarrow \text{FeOSO}_3^{1/2-} + \text{H}_2\text{O}$	(0.65,-1.65,0)	9.65
$\text{FeOH}^{1/2-} + \text{Ca}^{2+} \leftrightarrow \text{FeOHCa}^{1/2+}$	(0,32,1.68)	3.17
$2\text{FeOH}^{1/2-} + \text{Pb}^{2+} \leftrightarrow (\text{FeOH})_2\text{Pb}^+$	(1.2,0.8,0)	9.58 (99 %)
		12.25 (0.9 %)
		14.24 (0.1 %)
$2\text{FeOH}^{1/2-} + \text{Cu}^{2+} + \text{H}_2\text{O} \leftrightarrow (\text{FeOH})_2\text{CuOH} + \text{H}^+$	(0.5,0.5,0)	0.97
$2\text{FeOH}^{1/2-} + \text{Cd}^{2+} + \text{H}_2\text{O} \leftrightarrow (\text{FeOH})_2\text{CdOH} + \text{H}^+$	(0.5,0.5,0)	-1.42 (99 %)
		1.31 (1 %)
$2\text{FeOH}^{1/2-} + 2\text{H}^+ + \text{Pb}^{2+} + \text{PO}_4^{3-} \leftrightarrow (\text{FeO})_2\text{HPbPO}_3\text{H}^0 + \text{H}_2\text{O}$	(0.7,0.3,0)	33.64 (99 %)
		37.20 (1 %)
$2\text{FeOH}^{1/2-} + 2\text{H}^+ + \text{Cu}^{2+} + \text{PO}_4^{3-} \leftrightarrow (\text{FeO})_2\text{HCuPO}_3\text{H}^0 + \text{H}_2\text{O}$	(0.7,0.3,0)	31.71
$2\text{FeOH}^{1/2-} + 2\text{H}^+ + \text{Cd}^{2+} + \text{PO}_4^{3-} \leftrightarrow (\text{FeO})_2\text{HCdPO}_3\text{H}^0 + \text{H}_2\text{O}$	(0.7,0.3,0)	30.50

<sup>a</sup> The model is based on the interface parameters of Tibergh et al. (2013), and most of the values are from this reference, except for the Cd constants (Tibergh et al. 2016) and the SO<sub>4</sub> constant (Gustafsson et al. 2015). The Ca constant was optimised based on data given by Cowan et al. (1991).

<sup>b</sup> The change of charge in the *o*-, *b*- and *d*-planes respectively.

<sup>c</sup> Two or three numbers indicate binding to sites with different affinity, the percentages of which are within brackets (c.f. text).

<sup>d</sup> These values are based on a PZC of 8.1 and were adjusted in model simulations when PZC was increased (see text).

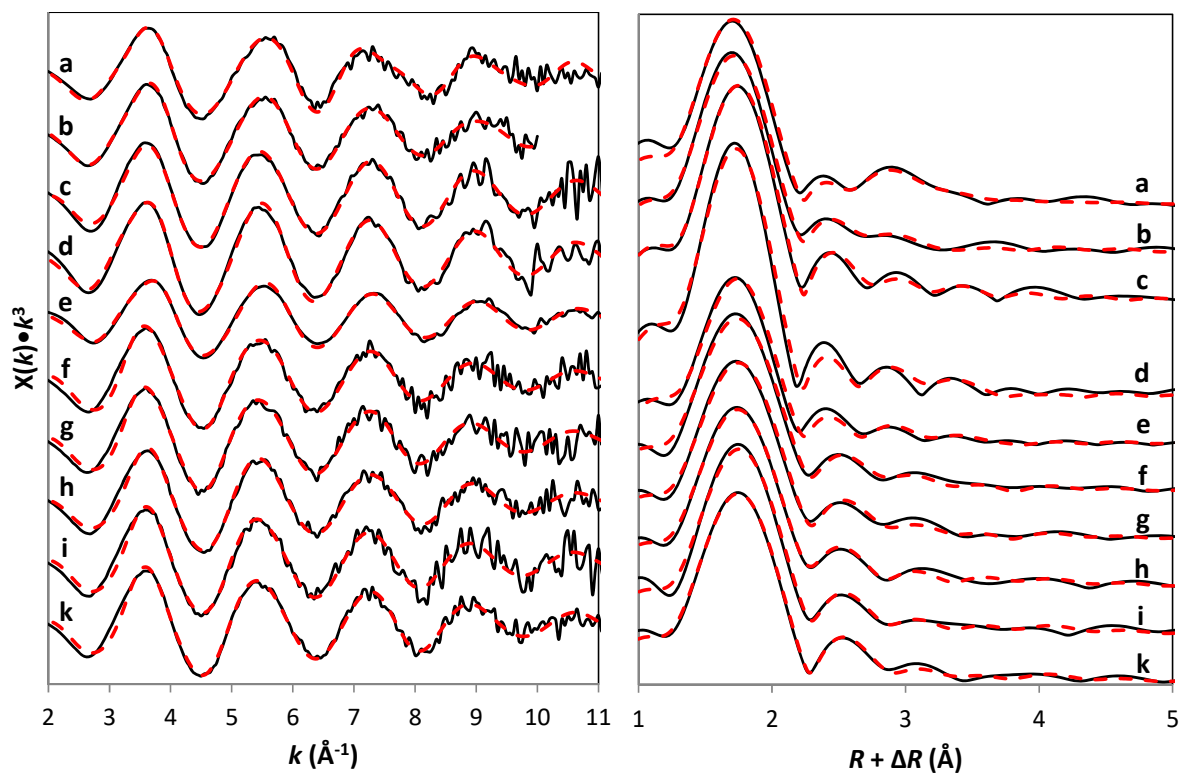


**Fig. S1.** Left: stacked  $k^3$ -weighted  $K$ -edge EXAFS spectra for cadmium for (a) Cd-Fh, (b) Cd-P-Fh, (c) Cd-FA, (d) Cd(II)(aq) 0.015, (e) Cd(II)(aq) 0.5, (f) Kloten 2 Cd, (g) Kloten 2 Cd+P, (h) Kloten 2 Cd+As, (i) Risfallet Cd, (k) Risfallet Cd+As (see Table 2 for descriptions). Black lines are raw data and red dashed lines are best fits. Right: Fourier Transforms (FT magnitudes) of the  $k^3$ -weighted EXAFS spectra.

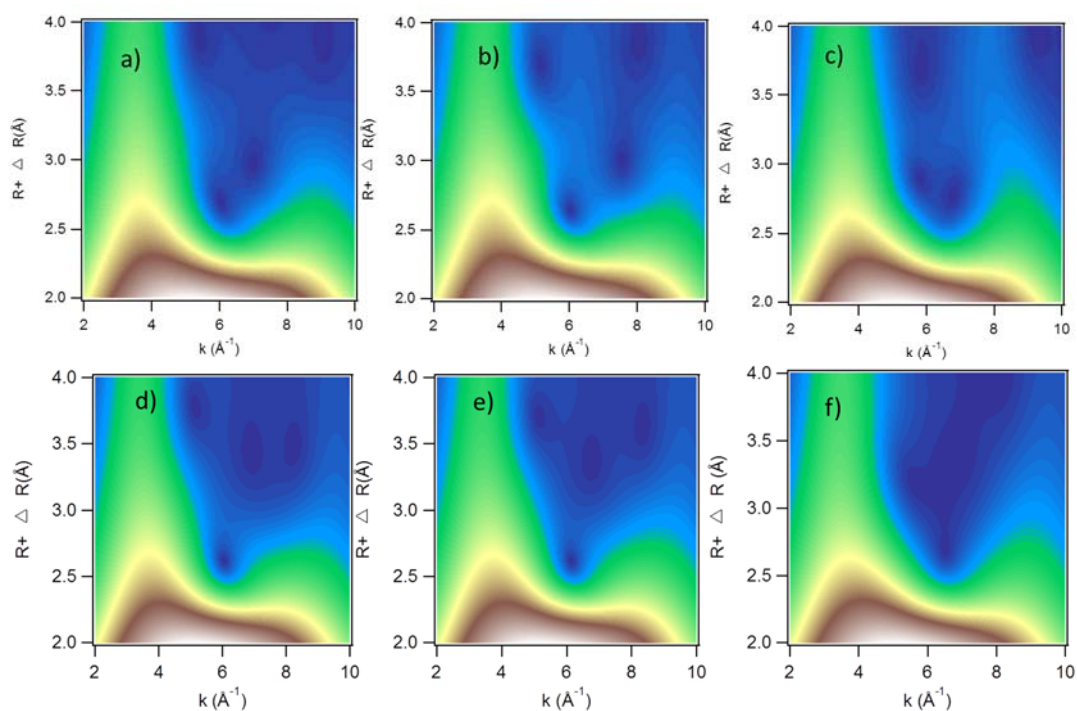


**Fig S2.** Wavelet transforms of Cd *K*-edge EXAFS spectra for the Kloten 2 samples. The *k*-range used was 3.5-9.5 Å<sup>-1</sup> for all samples. a) Raw spectrum, Kloten 2 Cd, b) Raw spectrum, Kloten 2 Cd+P, c) Raw spectrum, Kloten 2 Cd+As, d) Model Kloten 2 Cd, e) Model Kloten 2 Cd+ P, f) Model Kloten 2 Cd+As.

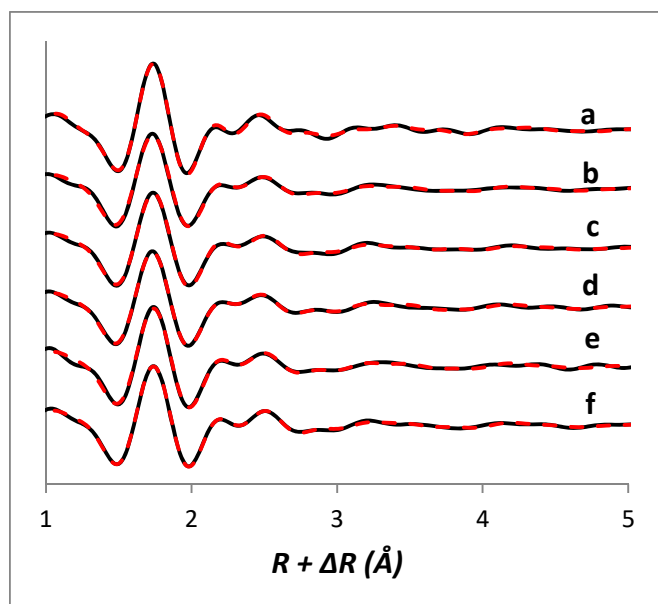


**Fig. S3.** Fourier Transforms (FT Real part) of  $k_3$ -weighted EXAFS spectra for (a) Cd-FA, (b) Kloten 2 Cd, (c) Kloten 2 Cd+P, (d) Kloten 2 Cd+As, (e) Risfallet Cd, (f) Risfallet Cd+As. Black lines are raw data and red dashed lines are best fits.

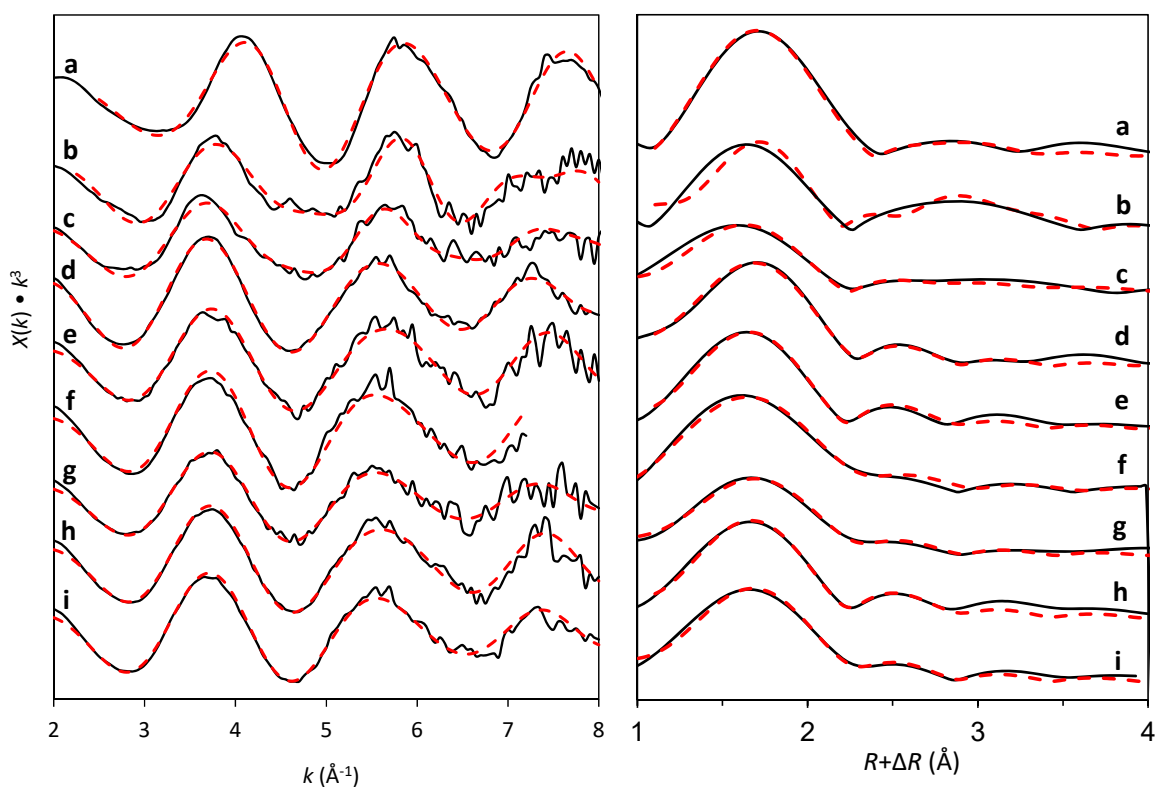


**Fig. S4.** Left: stacked  $k^3$ -weighted  $K$ -edge EXAFS spectra for lead for (a) Pb-Alox (b) Pb-Fh, (c) Pb-P-Fh, (d) Pb-FA, (e) Kloten Pb low, (f) Kloten Pb+P low, (g) Kloten Pb+As low, (h) Kloten Pb high, (i) Kloten Pb+P high (see Table 3 for descriptions). Lines are raw data and dashed lines are best fits. Right: Fourier Transforms (FT magnitudes) of the  $k^3$ -weighted EXAFS spectra.

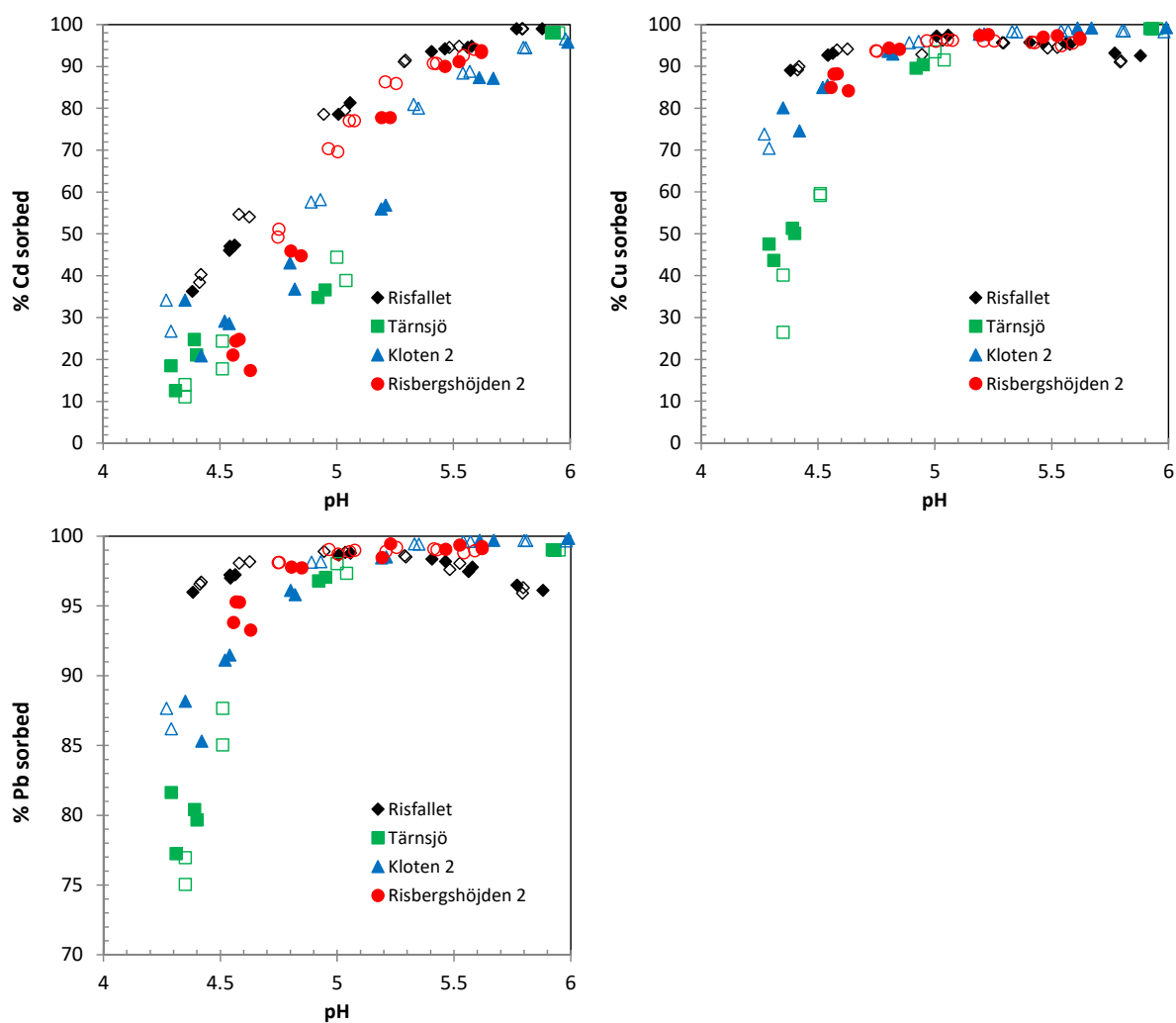


**Fig. S5.** Percent Cd, Cu and Pb adsorbed as a function of pH, with and without the addition of  $\text{PO}_4\text{-P}$  to an equilibrium concentration of  $1 \mu\text{M}$ . Filled and empty symbols represent samples with and without the addition of  $\text{PO}_4\text{-P}$ , respectively.

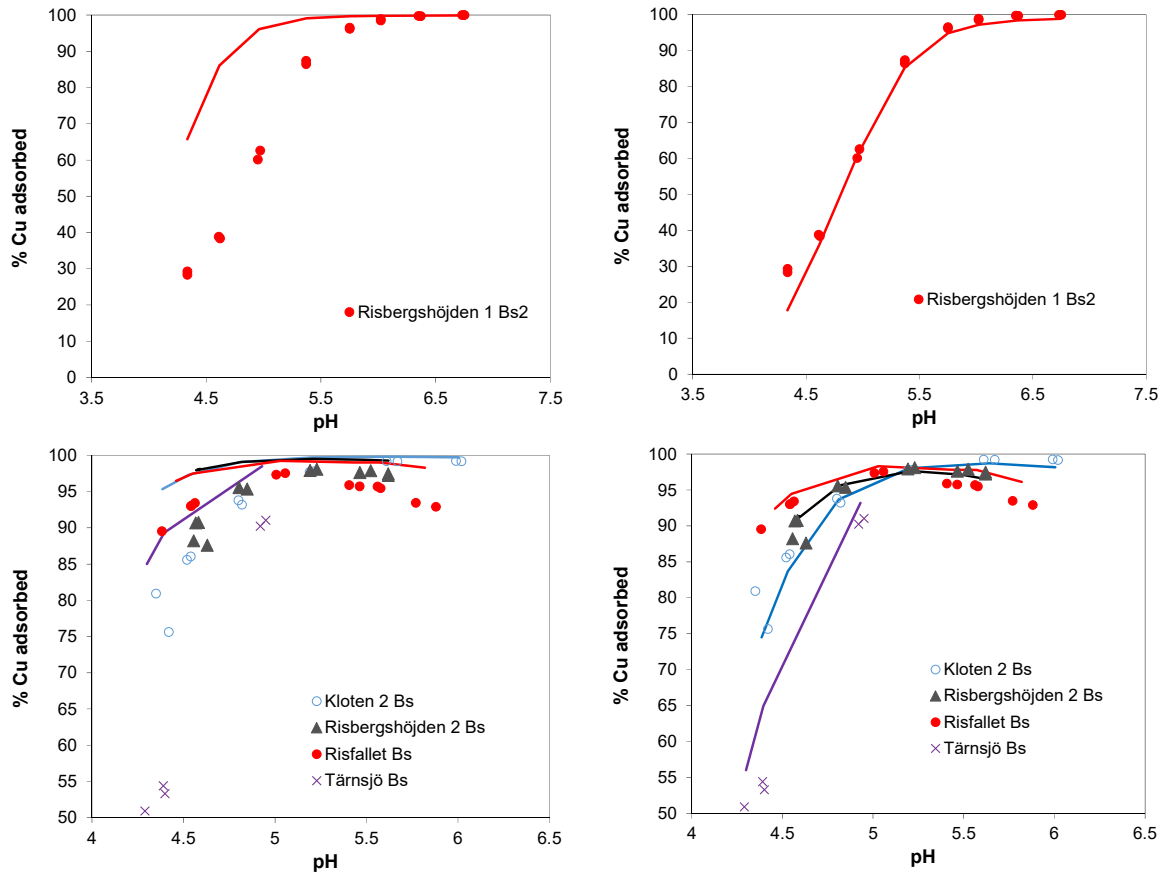


**Fig. S6.** Copper(II) adsorption as a function of pH. Points are observations and lines are model fits. Left column: Model fits assuming default parameters, i.e.  $f_{HS} = 0.55$  and  $PZC(Fh) = 8.1$ . Right column: Model fits with adjusted parameters (see Table 4).

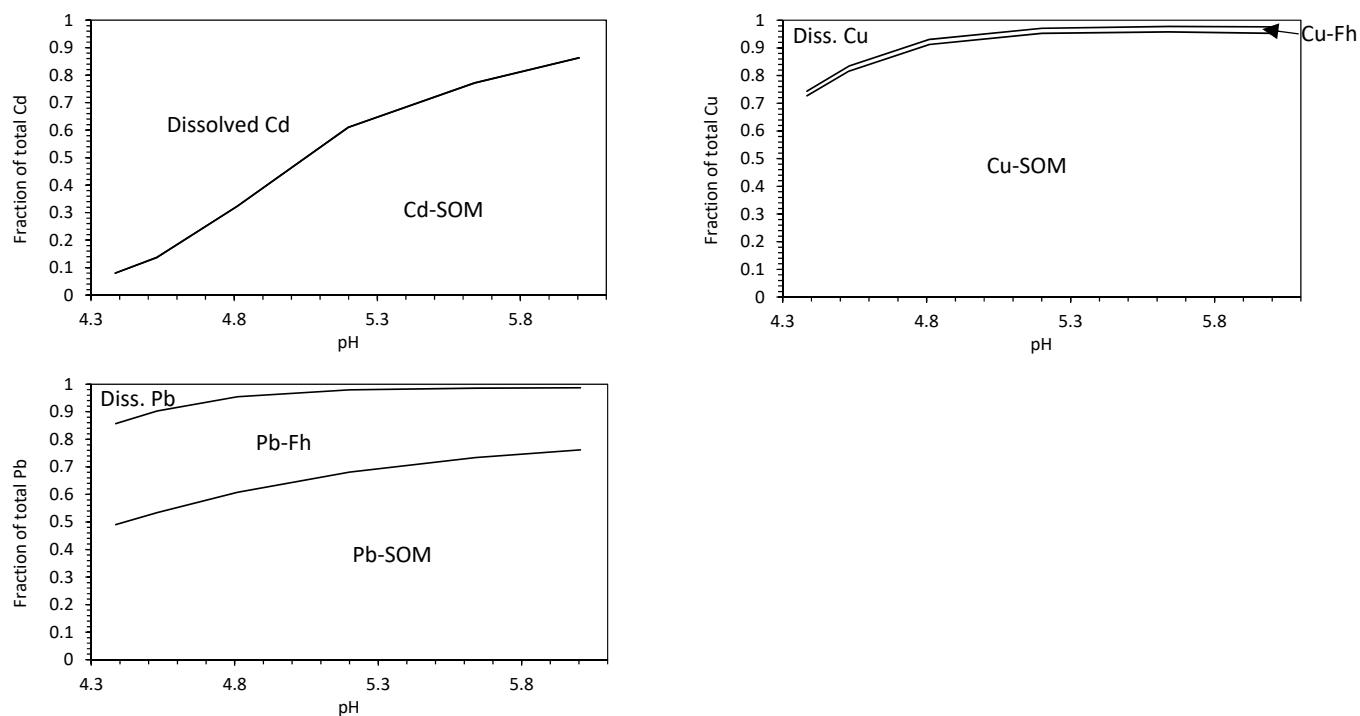


**Fig. S7.** Modelled relative contributions of cadmium(II), copper(II) and lead(II) bound to solid-phase organic matter (SOM) and to ferrihydrite (Fh) in the batch experiments with the Kloten 2 Bs sample (final model, shown in the lower right of Fig. 1, Fig. S6 and Fig. 2, respectively).

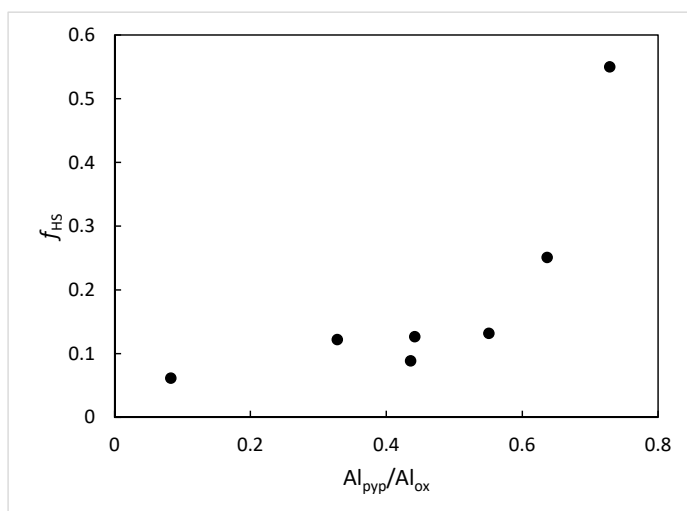


**Fig. S8.** The optimised value of the fraction active organic matter ( $f_{HS}$ ) as a function of the ratio of pyrophosphate-extractable Al to oxalate-extractable Al ( $Al_{pyp}/Al_{ox}$ ).

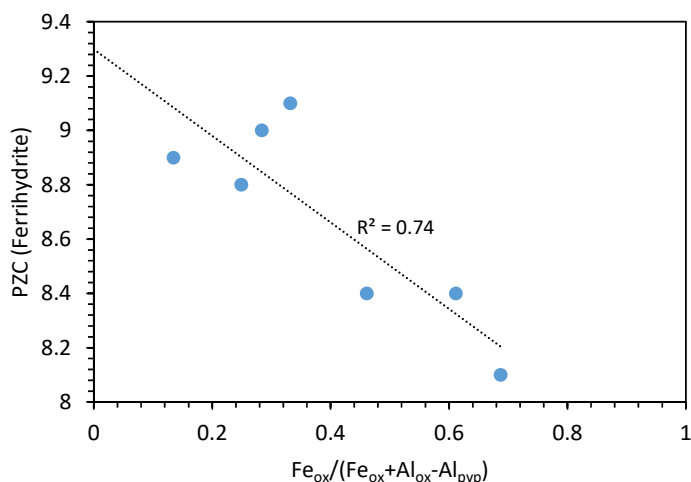


**Fig. S9.** The optimised PZC of soil ferrihydrite as a function of the fraction of poorly crystalline Fe oxide relative to the sum of poorly crystalline Fe + Al, as evidenced by the  $\text{Fe}_{\text{ox}}/(\text{Fe}_{\text{ox}}+\text{Al}_{\text{ox}}-\text{Al}_{\text{pyp}})$  ratio..

## References

- Cowan, C.E., Zachara, J.M., Resch, C.T., 1991. Cadmium adsorption on iron oxides in the presence of alkaline-earth elements. *Environ. Sci. Technol.* 25, 437-446.
- Gustafsson, J.P., Akram, M., Tiberg, C., 2015. Predicting sulphate adsorption/desorption in forest soils: evaluation of an extended Freundlich equation. *Chemosphere* 119, 83-89.
- Gustafsson, J.P., Kleja, D.B., 2005. Modeling salt-dependent proton binding by organic soils with the NICA-Donnan and with the Stockholm Humic models. *Environ. Sci. Technol.* 39, 5372-5377.
- Gustafsson, J.P., Pechova, P., Berggren, D., 2003. Modeling metal binding to soils: the role of natural organic matter. *Environ. Sci. Technol.* 37, 2767-2774.
- Gustafsson, J.P., Tiberg, C., Edkymish, A., Kleja, D.B., 2011. Modelling lead(II) sorption to ferrihydrite and soil organic matter. *Environ. Chem.* 8, 485-492.
- Linde, M., Öborn, I., Gustafsson, J.P., 2007. Effects of changed soil conditions on the mobility of trace metals in moderately contaminated urban soils. *Water Air Soil Pollut.* 183, 69-83.
- Tiberg, C., Gustafsson, J.P., 2016. Phosphate effects on cadmium(II) sorption to ferrihydrite. *J. Colloid Interface Sci.* 471, 103-111.
- Tiberg, C., Sjöstedt, C., Persson, I., Gustafsson, J.P., 2013. Phosphate effects on copper(II) and lead(II) sorption to ferrihydrite. *Geochim. Cosmochim. Acta* 120, 140-157.